



UNIVERSITY OF HELSINKI



<https://helda.helsinki.fi>

Using the Taguchi experimental design for assessing within-field variability of surface run-off and soil erosion risk

Raza, Ahsan

Elsevier Scientific Publ. Co

2022-07-01

Raza , A , Ahrends , H E , Habib-ur-Rahman , M , Hueging , H & Gaiser , T 2022 , ' Using the Taguchi experimental design for assessing within-field variability of surface run-off and soil erosion risk ' , Science of the Total Environment , vol. 828 , 154567 . <https://doi.org/10.1016/j.scitotenv.2022.154567>

<http://hdl.handle.net/10138/573340>

[10.1016/j.scitotenv.2022.154567](https://doi.org/10.1016/j.scitotenv.2022.154567)

cc_by_nc_nd

acceptedVersion

Downloaded from Helda, University of Helsinki institutional repository.

This is an electronic reprint of the original article.

This reprint may differ from the original in pagination and typographic detail.

Please cite the original version.

1 **Using the Taguchi experimental design for assessing within-field variability of surface run-**
2 **off and soil erosion risk**

3 **Ahsan Raza^{1,*}, Hella Ahrends², Muhammad Habib-ur-Rahman¹, Hubert Hüging¹ and Thomas Gaiser¹**

4 ¹**University of Bonn, Institute of Crop Science and Resource Conservation (INRES), Crop Science Group,**
5 **Katzenburgweg 5, 53115, Bonn, Germany**

6 ²**University of Helsinki, Department of Agricultural Sciences, 00014 Helsinki, Finland;**

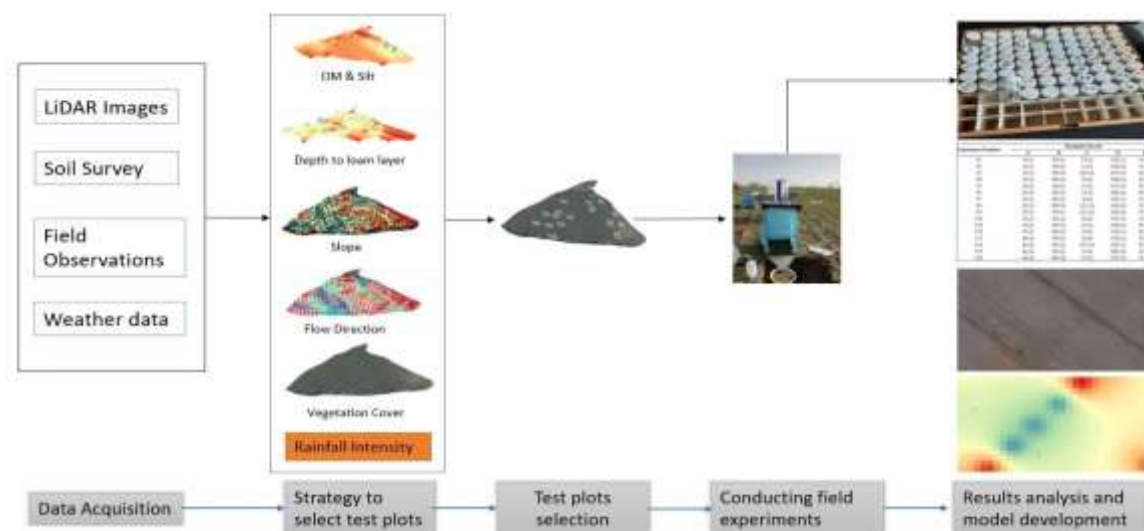
7 ***Correspondence: araza@uni-bonn.de; Tel.: +49(0)228 73-7200**

8 **Highlights**

- 9 • Taguchi’s Fractional factorial experiment design approach was used to rank the factors affecting
10 within-field soil erosion
11 • Signal-to-noise ratio analysis was used to identify optimum conditions for maximum sediment
12 yield, runoff, and carbon and nitrogen content of sediments.
13 • Rainfall intensity contributed most strongly to erosion processes with 40.6 % followed by
14 the slope (23.8 %).
15 • Applied workflow allowed for efficiently predicting soil erosion and identifying areas susceptible
16 to soil loss at a high spatial resolution

17

18 **Graphical abstract**



19

20 **Keywords:** Design of experiment, heterogeneous field conditions, rainfall simulator, erosion-prone areas

21

22

23 **Abstract**

24 Water erosion is one of the soil degradation processes driven by environmental and field factors
25 such as rainfall intensity, slope gradient, dynamics of vegetation cover, soil characteristics, and
26 management practices. Most of the studies assess the separate contribution of these factors under
27 controlled conditions. However, there is a lack of adequate knowledge regarding the complex
28 interactions between prevailing factors and soil erosion processes under heterogeneous field
29 conditions. This study investigated 16 combinations of 5 factors at 4 levels of each factor on the
30 soil erosion process using Taguchi's fractional factorial experiment design, identifying the factor
31 combinations resulting in maximum sediment yield, runoff, organic carbon, and nitrogen losses.
32 We considered the factors: Soil organic matter and silt content (SiltOM), vegetation cover (VC),
33 slope steepness (SS), rainfall intensity (RI), and depth to a loamy layer (DLL). The interactive
34 effects of these factors and their combinations were visualized from the analysis of signal-to-noise
35 (S/N) responses. Results indicated that interactions between the selected factors and soil erosion
36 processes exist and multiple linear regression models were developed to predict sediment yields,
37 runoff, carbon, and nitrogen losses at the sub-field scale. Results revealed that 1) RI with 40.6 %
38 showed the highest contribution to sediment yield followed by SS (23.8 %), VC (17.74 %), SiltOM
39 (14.77 %), and DLL (3.17 %), indicating a strong rainfall-erosion relationship; 2) the combination
40 of levels of factors generating highest sediment yield was determined; 3) A simple multiple linear
41 regression model developed for predicting local sediment yield showed the highest agreement with
42 field observations ($R^2=82.5$ %). The findings suggest that Taguchi design could be used reliably
43 for modeling soil erosion at field and sub-field scales. Using local calibration data such models
44 have great potential for soil erosion risk assessments at the field scale, especially in areas where
45 contributing factors and factor levels change at small spatial scales.

46

47

48

49

50

51

52 **1. Introduction**

53 Soil erosion by water has become a great concern all over the world (Keating et al., 2003;
54 Krysanova et al., 2007). Soil erosion has significant impacts on environmental sustainability by
55 adversely influencing agricultural production, water quality, and natural resources conservation
56 (Issaka and Ashraf, 2017). It reduces the fertile soil depth and crop available soil moisture by the
57 removal of essential nutrients and soil organic matter (SOM) and hence reducing the productivity
58 of the soil (Jahun et al., 2015). Soil erosion by water is a form of land degradation resulting from
59 multiple factors with complex interactions. Among others, these factors are rainfall intensity,
60 runoff, small-scale soil heterogeneity in the vertical and horizontal direction, topography, and
61 temporal variability of crop conditions (Václavík et al., 2013). Affected by heterogeneous
62 environmental and field conditions, soil erosion involves complex processes that can strongly vary
63 within single fields, in particular in undulated areas. (Cerdan et al., 2010). Therefore, identifying
64 and categorizing the main causes of soil erosion at the field scale based on observations with a high
65 spatial resolution for quantitatively assessing the spatial and temporal variability of soil erosion
66 patterns are of great importance. Such information can provide support for decision-making for
67 improved sub-field management and for farmers to avoid the degradation of fertile soils and for
68 maintaining or enhancing crop productivity.

69 Numerous experimental and modeling studies have been conducted using approaches ranging from
70 analytical to empirical techniques to gain a better understanding of runoff and soil erosion
71 processes (Raza et al., 2021) and their potential outcomes (organic carbon and nitrogen losses, soil
72 depth reduction, etc.) under heterogeneous field conditions (Aga et al., 2020; Eslamian, 2014; J.
73 R. Williams et al., 1984; Knisel and Nicks, 1981; Syvitski and Kettner, 2008; Viney and Sivapalan,
74 1999). Individual hydro-geomorphological processes and vegetation dynamics affect the soil
75 erosion process differently depending on the scale (Aga et al., 2020; Nearing et al., 1999; Panagos
76 and Katsoyiannis, 2019). In particular, soil physical properties such as soil structure, texture, bulk
77 density, compaction, and soil thickness influence the erosion pattern and thus rate and magnitude
78 of erosion (Ouyang et al., 2018; Ramezanpour et al., 2010). Other driving factors are the
79 topography (i.e., slope gradient, slope length) and ground cover, which modify the physical forces
80 and greatly impact hydrological processes (Liu and Singh, 2004). The amount, intensity, and
81 frequency of precipitation are critical meteorological factors for surface runoff generation and soil
82 erosion.

83 A few authors investigated the interactive impact of environmental and soil conditions on soil
84 erosion. (Guidry et al., 2006; Sepaskhah and Bazrafshan-Jahromi, 2006) investigated the runoff
85 and soil erosion under rainfall, varying slope, and soil factors, and found that the potentialities of
86 both surface runoff and sediment yield varied with the level of rainfall erosivity but the impact
87 differed among soil textures and slopes, indicating diverse nonlinearities of rainfall-runoff-soil
88 factors-erosion relationships and their complex interaction. (Zambon et al., 2021) studied the
89 dependency of soil erosion on soil surface conditions (seal formation) and soil types under
90 controlled rainfall intensities. Under the same initial surface conditions, the erosion development
91 for increasing rainfall intensity was almost consistent. (Warrington et al., 1989) noticed that
92 increasing slope inclination tends to increase erosion, whereas removing surface crusts and
93 increasing permeability rate led to decreasing surface runoff. (Gross et al., 1991) concluded that
94 even low density vegetation coverage noticeably decreases the sediment yield with increasing
95 rainfall intensities. However, different studies yield a different representation of erosion processes
96 Differences in the results of the studies are mainly caused by the particular experimental conditions
97 (selection of factors) and set-ups which affected the output. To date, there are a few attempts made
98 to study the impact of multiple environmental and in-field factors to predict sediment yield and
99 runoff, including, in some cases, carbon, and nitrogen losses under natural conditions (Anh et al.,
100 2014; Li et al., 2017; J. H. Zhang et al., 2015). Most of these studies consider only one (Cerdà et
101 al., 2021; Dunjón et al., 2004) or two (Ouyang et al., 2018; Ramos et al., 2019) factors to explain
102 the erosion process and ignore the complex interaction of potential factors and specifically their in-
103 field variability that may strongly affect the sediment yield and surface runoff. Most of these studies
104 used defined rainfall intensities at plot scales to investigate soil erosion using a rainfall simulator.

105 Rainfall simulators and soil erosion plots are two widely used research facilities to assess and
106 quantify the processes of soil erosion and sediment transport in overland flow (Sharpley and
107 Kleinman, 2003). Different types of rainfall simulators with their specifications and sizes being
108 optimized for specific pedo-climatic zones, topographies and land uses have been successfully
109 applied in several field experiments (Barthès and Roose, 2002; Duiker et al., 2001; Fernández-
110 Gálvez et al., 2008; Guidry et al., 2006; Lasanta et al., 2000; M. Sheklabadi et al., 2012; Sepaskhah
111 and Bazrafshan-Jahromi, 2006; Srinivasan et al., 2007). However, many of these studies used
112 standard plot sizes under controlled conditions (Albaladejo Montoro and Stocking, 1989; Raza et
113 al., 2021; Renard et al., 1991) and with rainfall intensities far higher than the threshold for soil

114 detachment thus neglecting the interactions of modulated intensities and soil characteristics that
115 can drive fine-scale spatial soil erosion processes (Kusumandari et al., 2021; Poulénard et al.,
116 2001). In summary, there is still a lack of knowledge on the interactive effects of multiple factors
117 and their potential levels on soil erosion processes under natural conditions that explicitly consider
118 sub-field scale spatio-temporal dynamics. The quantitative knowledge is however of great
119 importance for agricultural fields where management activities can lead to changes in the
120 vulnerability of soils to erosion. Spatially explicit knowledge will help to understand within-field
121 dynamics of erosion and sedimentation and greatly support precision agriculture by developing
122 physical-based on empirical-based models. . Further, it provides quantitative validation data for
123 high-resolution remote sensing data (such as unmanned aerial vehicle (UAV)-based Lidar
124 measurements).

125 Most of the previous studies were conducted under controlled conditions with a limited number of
126 factors, factor levels, and their interactions (Liu et al., 2019; Rieke-Zapp and Nearing, 2005;
127 Sadeghi et al., 2017; Yusuf et al., 2016). Observing multiple factors and their complex interactions
128 requires establishing several field experiments to disentangle their effects on spatial variation in
129 soil erosion. Therefore, these studies used full factorial experimental designs to investigate the
130 magnitude of the effects of factors on soil erosion that require a large sample size because it
131 increases exponentially when all combinations of factors, factor levels, and interactions are
132 considered (L. D. Meyer, 1981; Li et al., 2019; Meyer and Harmon, 1989). These designs are not
133 applicable when the number of experimental runs is limited due to their cost- and labor intensity.
134 To handle this challenge, the Taguchi method can be applied to any experimental study where the
135 effect of up to ~30 factors on processes is studied while labor and cost intensity are minimized
136 without lowering the quality of outputs (Taguchi, 1986). The Taguchi method is a type of general
137 fractional factorial design, based on a selected number of factors and factor levels to identify the
138 least number of experiments to be performed without compromising the overall output (Taguchi,
139 1987, 1986). So far, in an agricultural context, the Taguchi design mainly has been used for
140 investigating the impact of fertilizer rates and plant density on cotton yields (Awty-Carroll et al.,
141 2020; Chou et al., 2010; Ruchika Deo et al., 2007; Sivaiah & Chakradhar, 2019b). Further, it has
142 been successfully applied to study soil erosion processes (Sadeghi et al. 2012, Mhaske et al. 2019)
143 and results indicate similar performance compared with full factorial designs (Zhang et al. 2015,
144 Zhang et al. 2021) and response surface methods (Moosavi & Sadeghi. 2021(F. Zhang et al.,

145 2015)). While providing evidence for the suitability of the design to study the effect of multiple
146 factors on soil erosion, these studies only used a limited number of factors and their interactions.
147 Further, runoff volume and resulting nutrient losses such as organic carbon and nitrogen from the
148 field, which are critical variables for sustainable agriculture, were not investigated.

149 Encouraged by the successful application of this design in the studies mentioned above, we here
150 use the Taguchi design to study fine-scale spatio-temporal dynamics of soil erosion processes
151 (surface runoff, sediment yield, carbon and nitrogen losses) as affected by multiple factors at an
152 agricultural field located in Western Europe under temperate climate conditions. More specifically,
153 the objectives of this study are to

- 154 i. Investigate the within-field variability of the effects of the interaction between soil
155 characteristics (soil organic matter (SOM), soil texture), topography (slope), rainfall
156 intensity, and soil cover (field conditions) on soil erosion, surface runoff, carbon and
157 nitrogen losses
- 158 ii. Quantify the percentage contribution of each of these five factors to soil erosion, surface
159 runoff, carbon and nitrogen losses
- 160 iii. Develop empirical models to predict local runoff, sediment yield, carbon and nitrogen
161 losses
- 162 iv. Identify erosion risk and sediment yield zones within the field

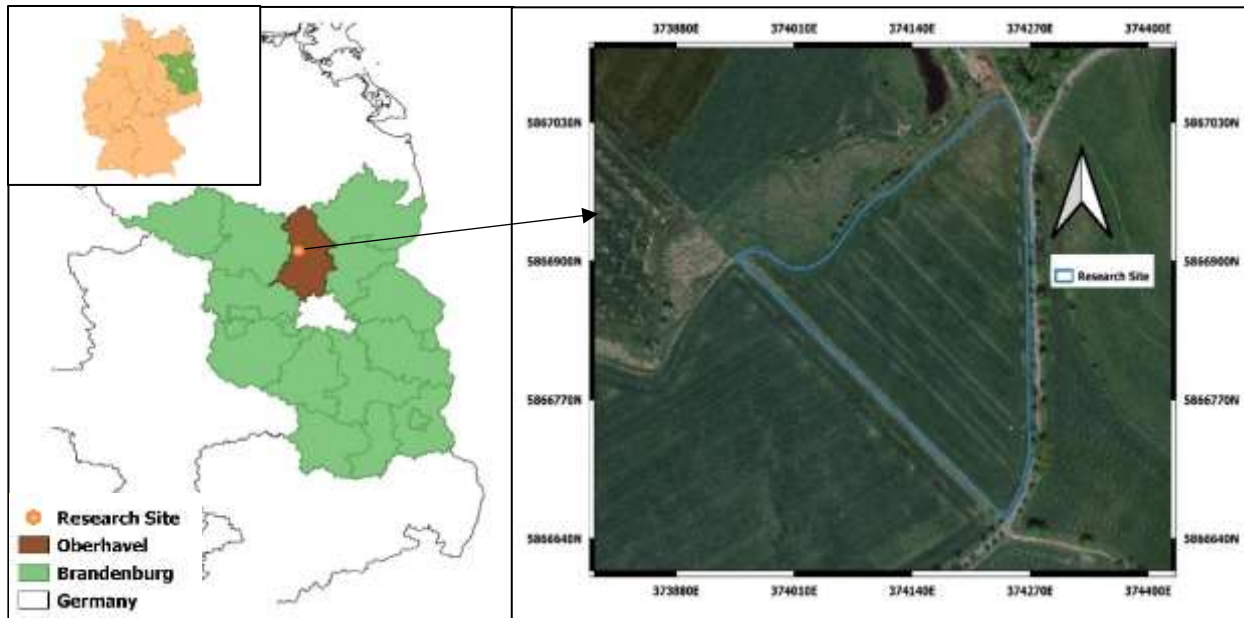
163 **2. Methodology**

164 2.1. Study area

165 The study was conducted on an agricultural field site located in the Löwenberger Land
166 municipality, in the north of the federal state of Brandenburg, Germany (33U 374170E 5866893N)
167 (Fig. 1). Brandenburg lies in the temperate, continental climate zone with mean annual
168 temperatures between 7.8 °C and 9.5 °C and mean annual precipitation of ~ 600 mm (German
169 Weather Service 2020, Ihinegbu & Ogunwumi, 2021). The research field comprises ~ 6.25 ha (Fig.
170 1). Terrain height averages around 51.5 to 57.5 m a.s.l. with north east facing gentle slope (Fig.
171 2). The soil was classified as Ferric Luvisol at up slopes (WRB, 2007) and in the marginal areas of
172 the depression as Gley-Kolluvisol (Gleyic Anthrosol).

173

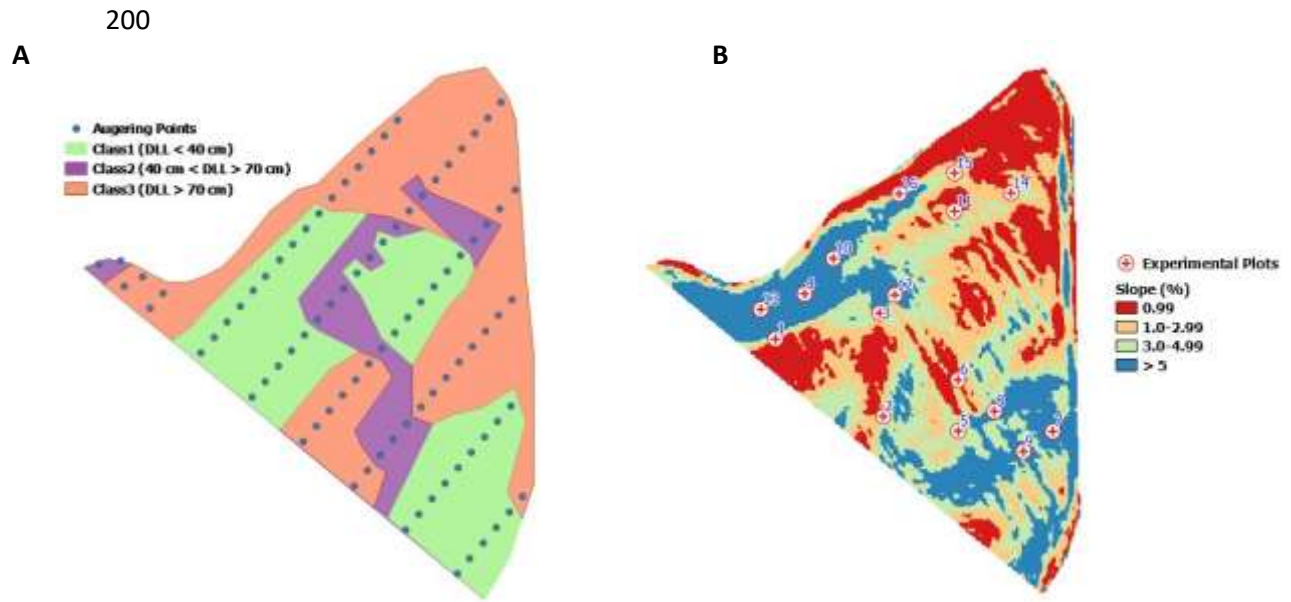
174



185 **Fig. 1: Location of the study area (left) and an aerial image of the research field (May 8th,**
 186 **2020, Google Earth)**

187 2.2. Soil sampling

188 To characterize the spatial heterogeneity of soil characteristics soil augers (100 cm depth) were
 189 obtained from 87 different locations within the field (Fig. 2) in December 2019. At selected points,
 190 soil samples were analyzed for soil texture (proportion of silt, sand, and clay fractions) and SOM
 191 content, and the depth from the soil surface to a loamy layer. In soils derived from glacial deposits,
 192 the thickness of the sandy topsoil layers that are followed by a loamy layer, restricting vertical
 193 water movement compared to the sandy topsoil, is considered to increase the risk of water ponding
 194 at the soil surface and hence the risk of surface runoff and erosion. Samples were air-dried and
 195 sieved through a 2 mm mesh. Particle size distribution was determined with the Pipett method after
 196 SOM and carbonate destruction. Soil texture varied from silty loam to silt and medium sand
 197 according to the German soil taxonomy. According to Hofmann et al. (2016) and the soil taxation
 198 values in the German field cadastre of the state of Brandenburg (BB ATKIS), however, the topsoil
 199 is dominated by loamy sand.



201 **Fig. 2: Study site with soil augering points (A) and the locations of the rainfall simulation**
 202 **experimental plots (B, Numbers 1 to 16)**
 203

204 2.3. Experimental design

205 In contrast to classical statistical designs the “Taguchi design” is a type of general fractional
 206 factorial design, based on a selected number of factors and factor levels to identify the least number
 207 of experiments to be performed (Taguchi, 1987, 1986). The main factors and interactions that are
 208 most likely to be significant and the levels at which they are varied have to be defined in advance.
 209 Based on this knowledge Taguchi orthogonal arrays are selected with the choice depending on the
 210 tradeoff between time, resources, and quality of outputs (Medan et al., 2017; Rafidah et al., 2014;
 211 Woll & Burkhard, 2005). Subsequently to the experimental runs, the effect of each variable can be
 212 studied based on the signal-to-noise ratio (SN) (i.e., maximizing or minimizing SN ratios).

213 The Taguchi method systematically yields the best possible combination of factors and their levels
 214 to produce quality output at lower experimental cost and time. Based on the literature review
 215 (Chmelová and Šarapatka, 2002; P.U. et al., 2017; Pandey et al., 2007; Raza et al., 2021), For this
 216 study, five factors were selected: Sum of the percentage of silt and soil organic matter (SiltOM),
 217 vegetation cover (VC), slope steepness (SS), rainfall intensity (RI), and depth to loamy layer
 218 (DLL). For each factor, four levels are considered (Table 1). The ranges of these levels are based
 219 on soil surveys, site-specific scheduling of crop residue management (affecting vegetation cover),
 220 and the field topography derived from 2008 Lidar data with 1m spatial resolution

221 (<https://geobroker.geobasis-bb.de>). The selection of rainfall intensity levels is based on an analysis
 222 of 10-minute precipitation data provided by the German Weather Service for a nearby
 223 meteorological station (Brandenburg weather station (ID # 3552)) and adjusted to the capability
 224 and sensitivity of the mobile rainfall simulator (described below).

225 **Table 1: Experimental factors and their levels**

Factor	Description	Unit	Level 1	Level 2	Level 3	Level 4
1	(SiltOM)*	%	> 20	18 - 20	16 - 18	< 16
2	vegetation cover	%	1 - 5 (C)	0 (B)	10 - 15 (E)	> 15 (L)
3	Slope steepness	%	< 1	1-3	3-5	> 5
4	Rainfall intensity	mm min ⁻¹	< 2.5	2.7 - 3.3	3.4 - 4	> 4
5	Depth to loamy layer	cm	< 40	40 - 55	55 - 70	> 70

226 *the % of SiltOM decreases from level 1 to level 4, decided based on laboratory soil texture
 227 analysis. C, B, E, and L represent field conditions as cultivation, seedbed preparation, plant
 228 emergence, and Leaf development stage (3 Leaves unfold) respectively.

229 Due to the number of factors (5) and levels (4) as defined in Table 1, the orthogonal array L₁₆ (4⁵)
 230 for the Taguchi DOE was selected consisting of 16 experiments (factor combinations) (Table 2).

231

232

233

234

235

236

237

238

239

240

241

242

243

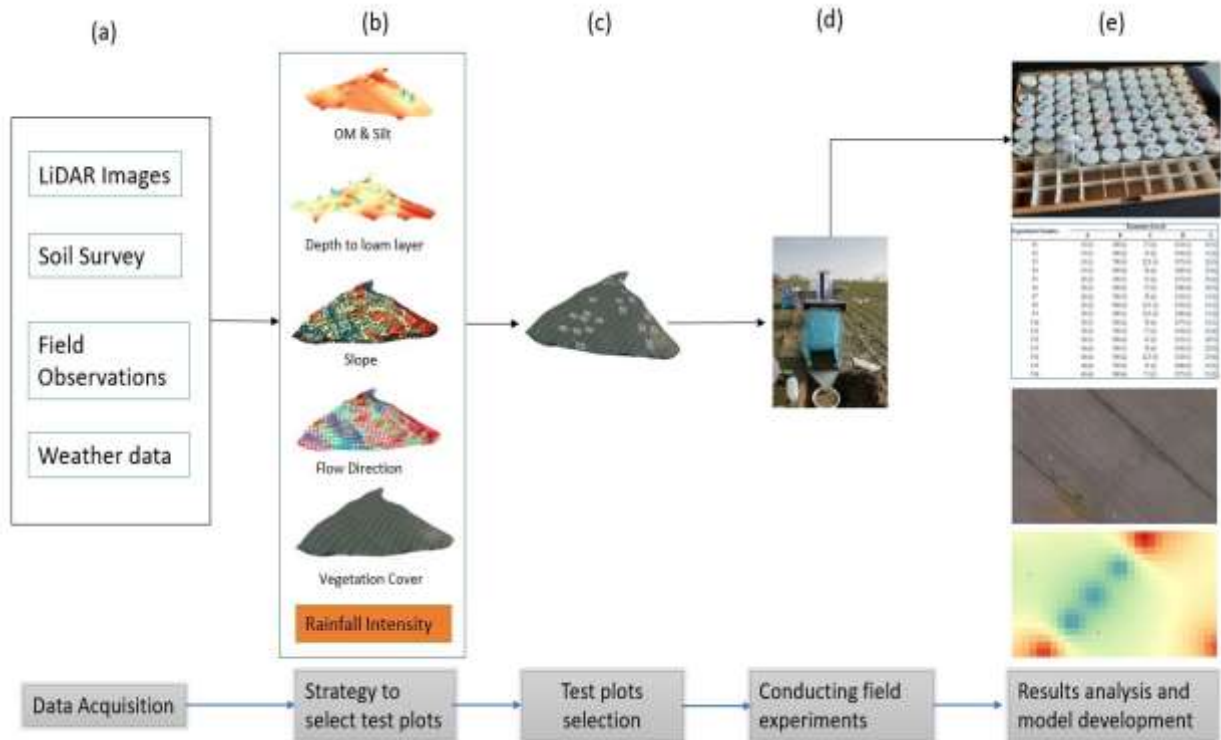
Table 2: Taguchi fractional factorial design L16 (4⁵) used in this study

Factors \ Plot ID	Combination of levels					SiltOM (%)	Vegetation cover (%)	Slope steepness (%)	Rainfall intensity (mm min ⁻¹)	Depth to loamy layer (cm)
	1	2	3	4	5					
1	1	1	1	1	1	>20	1-5	<1	<2.5	<40
2	1	2	2	2	2	>20	0	1-3	2.7-3.3	40-55
3	1	3	3	3	3	>20	10-15	3-5	3.4-4	55-70
4	1	4	4	4	4	>20	>15	>5	>4	>70
5	2	1	2	3	4	18-20	1-5	1-3	3.4-4	>70
6	2	2	1	4	3	18-20	0	<1	>4	55-70
7	2	3	4	1	2	18-20	10-15	>5	<2.5	40-55
8	2	4	3	2	1	18-20	>15	3-5	2.7-3.3	<40
9	3	1	3	4	2	16-18	1-5	3-5	>4	40-55
10	3	2	4	3	1	16-18	0	>5	3.4-4	<40
11	3	3	1	2	4	16-18	10-15	<1	2.7-3.3	>70
12	3	4	2	1	3	16-18	>15	1-3	<2.5	55-70
13	4	1	4	2	3	<16	1-5	>5	2.7-3.3	55-70
14	4	2	3	1	4	<16	0	3-5	<2.5	>70
15	4	3	2	4	1	<16	10-15	1-3	>4	<40
16	4	4	1	3	2	<16	>15	<1	3.4-4	40-55

244

245 2.4. Plot selection

246 To select plot locations for experimental runs covering each of the 16 factorial combinations (Table
247 2), field maps on the depth to a loamy layer, slope inclination, and the sum of silt and OM were
248 prepared, using SAGA within QGIS 3.16 (Fig. 3). Data on the depth to a loamy layer was derived
249 from field surveys. Point data were spatially interpolated using ordinary kriging in SAGA. The
250 topography was derived from 2008 LiDAR imagery (<https://geobroker.geobasis-bb.de>).
251 Subsequently, map overlays were used to identify 16 plot locations. The 16 locations were
252 considered to be well distributed in the research site (Fig. 2). At each location, rainfall simulator
253 experiments were carried out at the respective intensity levels with 4 repetitions. To integrate the
254 factors “vegetation cover”, simulations were performed on multiple dates with vegetation cover
255 ranging from 0% (seedbed preparation), over 5% (cultivation) and 10% (crop emergence, DAS:
256 20) to >15% (leaf development stage 3, DAS: 204) (Table 3).



257

258 **Fig. 3. Schematic diagram of the workflow for the rainfall simulation experiment: (a)**
 259 **Preprocessing of soil samples and remote sensing data (b) Preparing within-field factor levels**
 260 **for the Taguchi design (c) Selecting the locations of experimental plots (d) collecting**
 261 **sediments and runoff (e) Filtering and weighing sediment samples, runoff and CN**
 262 **concentration in sediments**

263

264 2.5. Rainfall simulator

265 In this study, in order to generate targeted levels of rainfall intensity (Table 2), the portable non-
 266 pressurized rainfall simulator (Kamphorst, 1987) was used (Fig. 3d). The simulator was produced
 267 by Eijkelkamp (Eijkelkamp Agrisearch Equipment, Netherlands) and the design is owned by
 268 Wageningen University Research Centre. The ground coverage area is 0.0625 m² enclosed from
 269 three sides with stainless steel frame. The basic unit of the simulator consists of two Plexiglas
 270 containers connected with the frame. The upper container has a calibrated cylindrical reservoir
 271 having a capacity of 2300 ml. The lower container has 49 capillaries with a diameter of 0.6 mm.
 272 The basic unit is supported with four adjustable legs, 0.4 m average in height, on various slopes.
 273 Rainfall intensity is controlled by varying the atmospheric pressure inside the basic unit through
 274 an adjustable aeration pipe attached to the upper container. Fig. 3d illustrates the operation of the
 275 rainfall simulator in the field. Before the beginning of the experiments, the rainfall simulator was

276 calibrated in order to generate the four different rainfall intensities (Table 2) (Kamphorst, 1987;
277 “Rainfall simulator - Field measurement equipment | Eijkelkamp,” 2018). Each experiment was
278 carried out for the duration of 8 minutes keeping in view the storage capacity of the reservoir and
279 rainfall intensity levels. However, for the rainfall simulator, it is recommended to use it at the
280 wettest season i.e., soil moisture content near to field capacity, when the soil surface is most
281 vulnerable to erosion. For that purpose, a pre-wetting of the plot was carried out in the dry season.
282 The water for pre-wetting is carefully applied through a plastic container with a perforated lid on
283 it to avoid splash and runoff.

284 2.6. Sample preparation

285 The runoff from each plot and repetition and the corresponding sediment yields were collected in
286 a 2L plastic bucket installed at the downslope end of the stainless steel frame of the simulator. The
287 samples were thoroughly mixed by stirring before transferring them into plastic bottles. The
288 volume of samples (runoff + sediment) was determined using glass flasks in the laboratory
289 followed by wet sieving through a sieve with a mesh size of 2 mm. The samples were then placed
290 in the oven at 60 °C for drying the dried samples and were later weighted to determine the sediment
291 yield. There were no stones > 2 mm collected in any of the samples. A pycnometer with distilled
292 water was used to determine the volume of sediments collected from each experimental plot
293 (Benjeddou et al., 2017; Heiskanen, 2008). Surface runoff volume was calculated by subtracting
294 the sediment volume from the total sample volume collected in the field. The sediment samples
295 were then dried at 60 °C till samples were fully dried to prepare them for carbon and nitrogen (CN)
296 analysis. The dried samples were transferred then into separate glass scintillation vials and analyzed
297 for CN content by instantaneous oxidation of the sample via combustion with oxygen at an
298 approximate temperature of 1020° C using an Elemental Analyzer Euro EA 3000 (EuroVector -
299 RK Tech Ltd., Pavia)

300 2.7. Statistical analysis

301 In Minitab 17.0 software tool, signal-to-noise ratio analyses (SN) were used for the evaluation of
302 experiment results (Chou et al., 2010; Sivaiah and Chakradhar, 2019). Three types of SN ratios are
303 used (1) Nominal is better, (2) Higher is better, (3) Lower is better. Because the objective of this
304 study is to identify the areas with the highest risk of erosion, “the higher the better (HB)” approach
305 was used. The following equation was used to calculate the SN-ratio:

306
$$\frac{S}{N_s} = -10 * \log \left(\frac{1}{n} \sum \frac{1}{y^2} \right) \quad (1)$$

307 where, n represents the number of repetitions at each rainfall simulation plot, and y represents the
 308 studied variable. Here, y is sediment yield, runoff, nitrogen, or carbon content in the sediments
 309 from each experimental plot.

310 The statistical approach of analysis of mean (ANOM) was used to derive optimal conditions (Parr
 311 and Taguchi, 1989). ANOM is a graphical method for multiple group comparisons with an overall
 312 mean (“grand mean”). The mean $\frac{S}{N_s}$ ratio of each factor I at a specific level i (Eqn. 2) was
 313 determined using the following equation:

314
$$M_{Factor}^{Level} = \frac{1}{n_{ii}} \sum_{j=1}^{n_{ii}} \left[\left(\frac{S}{N_s} \right)_{Factor = I}^{level = i} \right]_j \quad (2)$$

315 In equation (2), n_{ii} is the number of occurrences of factor I in level i . $\frac{S}{N_s}$ response figures and tables
 316 were obtained, and optimum conditions were established for each concerning output. J?

317 In addition, an analysis of variance (ANOVA) was used to investigate the influence of individual
 318 factors on sediment yield, runoff, and CN content (Cox et al., 2008). The percentage contribution
 319 of each experimental factor to the four output variables was estimated using the following equation:

320
$$\rho_F = \frac{SS_F - (DOF_F V_{ER})}{SS_T} \times 100 \quad (3)$$

321 Where V_{ER} is the variance of error, SS_F is the factorial sum of squares, and DOF_F represents a
 322 degree of freedom obtained by subtracting one from the number of levels of each factor (L). The
 323 total sum of squares, SS_T , was calculated using the following equation:

324
$$SS_T = \sum_{j=1}^m \left(\sum_{i=1}^L Y_i^2 \right)_j - mn(\bar{Y}_t)^2 \quad (4)$$

325 Y_t is obtained as:

326
$$\bar{Y}_t = \sum_{j=1}^m \left(\sum_{i=1}^L Y_i \right)_j / mn \quad (5)$$

327 Where, m represents the number of experimental plots covered in this study, and n represents the
 328 number of repetitions under the same experimental plot. The factorial sum of squares, SS_F , is given
 329 by:

$$330 \quad SS_F = \frac{mn}{L} \sum_{k=1}^L (\bar{Y}_K^F - \bar{Y}_t) \quad (6)$$

331 \bar{Y}_K^F is the average value of the measurement results of a certain factor in the k th level. Furthermore,
 332 the variance of error, V_{ER} was given by:

$$333 \quad V_{ER} = \frac{SS_T - (\sum_{F=A}^D SS_F)}{m(n-1)} \quad (7)$$

334

335 **3. Results and discussion**

336 **3.1. Sediment yield**

337 The variation of sediment yield depending on the five factors and their levels is shown in Fig 4A
 338 and 5A respectively. The average amount of sediment yield across replicates varies from $499.2 \pm$
 339 20.6 to 60.5 ± 17.3 g m⁻². Plot-based rainfall simulation data show pronounced relative differences
 340 in sediment yield among different combinations of factors and their respective levels (Fig. 4A).
 341 Experimental plot B10 (0 % vegetation cover, a rainfall intensity of 3.4-4 mm min⁻¹, the slope of 4
 342 %, SiltOM 16-18% of and DLL of < 40cm) shows the highest sediment mass with 499.2 g m⁻²,
 343 indicating the highest erosion levels under these conditions. The lowest sediment mass (60.5 g m⁻
 344 ²) was obtained at plot L12 (vegetation cover was >15 %, rainfall intensity < 2.5 mm min⁻¹, and
 345 slope between 1 and 3 %). Fig 5 shows the means of sediment yield for each factor and each level
 346 and compares them to the overall factor mean (grand mean, dashed line) (ANOM). These graphs
 347 show that the amount of sediment increases with an increase in rainfall intensity (Fig. 5A). The
 348 minimum rainfall intensity needed to initiate soil erosion, in this study, was 2.5 mm min⁻¹. At lower
 349 rainfall intensities, the infiltration rate is higher in the beginning. The potential kinetic energy of
 350 raindrops is small and the splash effect is weak and so is the sediment yield. In addition, runoff
 351 volume is relatively small under lower rainfall intensities (Mohamadi and Kaviani, 2015). The
 352 relationship between rainfall intensity and sediment yield varied across intensity levels in a
 353 systematic way (Fig. 5A). The sediment yield increased to 204.9 g m⁻² when the RI increased to
 354 level 2, which was 73.5 g m⁻² higher than at RI level 1. The increment was 253.3 g m⁻² and 310.7
 355 g m⁻² with RI levels 3 and 4 respectively, where sediment yields were respectively 1.9 and 2.4
 356 times higher than at RI level 1 (Fig. 5A). This result may indicate that at the plot scale, soil loss

357 would linearly increase up to a threshold of rainfall intensity, beyond which soil loss would increase
358 non-linearly. Similarly, (Kandel et al., 2004) found a non-linear relationship between high-intensity
359 rainfall and soil erosion processes. Therefore, it can be suggested that high rainfall intensities
360 resulted in greater soil losses. This is also confirmed by other studies where high intensity rainfall
361 events increased sediment yield (Jebari et al., 2008; Sukartaatmadja et al., 2003; Ziadat and
362 Taimeh, 2013a) and sediment transport.

363 Soil detachment and runoff significantly increased with rainfall intensity for both uncultivated and
364 cultivated lands (Ziadat and Taimeh, 2013b) but the level of vegetation cover has a significant
365 effect on the soil detachment. As for plot B10, the same rainfall intensity of $3.4\text{--}4\text{ mm min}^{-1}$ was
366 applied to plots E3, C5, and L16 producing 188.1 g m^{-2} , 207 g m^{-2} , and 199 g m^{-2} average sediment
367 yield respectively (Fig. 4). However, in plot B10 the sediment yield was 499.2 g m^{-2} . Among the
368 rates of sediment yield for four vegetation covers analyzed in this study, vegetation cover level 4
369 was found most beneficial for preventing soil losses. The eroded sediment yield was below 149 g
370 m^{-2} when the vegetation cover was more than 15 % (level 4). The sediment yield generally tended
371 to decrease with an increase in vegetation cover (Table 3). The highest mean sediment yield
372 (averaged across all other factors) was observed after seedbed preparation (vegetation cover 0 %)
373 with 292.16 g m^{-2} (Fig. 5A). In this study, increasing vegetation cover dramatically reduces
374 sediment yield which is in accordance with the results of (Donjadee and Chinnarasri, 2012; Lin et
375 al., 2018). (Zapata et al., 2021) mentioned that the vegetation cover interception reduces the
376 diameter of the drops reaching the soil surface and hence reduces the kinetic energy of a raindrop.
377 (Huang et al., 2012) also described that vegetation cover increases soil surface roughness that acts
378 as a barrier to impede surface runoff and increases infiltration time. Thus, vegetation cover reduces
379 the sediment yield by reducing the kinetic energy of raindrops, intercepting rainfall, increasing
380 surface roughness, and enhancing infiltration times.

381 A positive relationship was further detected between slope and sediment yield. The sediment yield
382 increased from 162.24 g m^{-2} at a slope of 1 % to 297.44 g m^{-2} at a slope of 5 % Fig. 5A. Previous
383 studies also show that the sediment yield increases with increasing slopes. This indicates a strong
384 positive relationship between slope and sediment yield (Grismer, 2012). Under extreme rainfall
385 intensities, it has been observed that surface runoff velocity and sediment yield are primarily driven
386 by slope inclination (Yan et al., 2018). These observations are likely related to higher overland
387 flow velocities at higher slope gradients (Defersha and Melesse, 2012) resulting in higher sediment

388 yield. A gentle slope is less subject to activation and transportation of eroded sediments.
389 Additionally, the splashing effect of raindrops generates surface sealing on gentle slopes producing
390 more surface runoff carrying sediments. Soil particles are detached from the steep slopes where
391 downward gravity is comparatively large. Therefore, there is a tradeoff between rainfall intensity
392 and slope gradient. (Wu et al., 2018b) proved that rainfall intensity has more influence than slope
393 gradient on sediment yield.

394 The surface soil texture also governs the sediment yield under varying rainfall intensity events.
395 Water availability and water holding capacity are largely dependent on the texture of the soil
396 profile, especially under rain-fed conditions (Libohova et al. 2018; Wang et al. 2020; Zhou et al.
397 2020). The decreasing concentration of SiltOM in the surface soil showed an increasing trend in
398 sediment yield except for level 4 (2.5 %) which produced a mean sediment yield of 263.52 g m^{-2}
399 which was slightly lower than at level 3 (275.84 g m^{-2}). The detachment of soil is mainly affected
400 by the size and weight of soil particles, organic matter, and the kinetic energy of the raindrops
401 (Sadeghi et al., 2017). The silt content varies from 10.2 to 19.5 % in the study area. The loose
402 particles of silt showed a higher tendency to detachment and erosion process. Soil erodibility
403 increases with increasing silt content (Baruah et al., 2019) but it reduces drastically once the crust
404 is formed. However, SiltOM explicated the strong negative effects of mean weight diameter on
405 splash erosion, and the indirect impact of high organic matter ($> 2\%$) on splash erosion by
406 improving the aggregate stability (Sun et al., 2021). Moreover, With high rainfall intensity and
407 longer test duration, detaching capacity was achieved faster and a surface seal appeared on the soil
408 surface (Michel et al., 2014).

409 3.2. Surface runoff

410 At different growth stages of the crop, the runoff process at different rainfall intensities, slope
411 gradients, and soil textures are shown in Fig. 4B. The observed mean runoff volume varies between
412 23.5 ± 1.07 and 6.54 ± 0.62 mm among the plots. The plots where rainfall intensity level 4 was
413 applied showed 42.5 % more surface runoff compared to those plots with rainfall intensity level 1.
414 The increase of runoff in the low rainfall intensities was gentle and later it tend to be large. In
415 general, for the highest rainfall intensity, the recorded runoff depth varied from 23 mm to 17.2 mm.
416 On the other hand, for the events with the lowest rainfall intensity, the recorded runoff depth varied
417 from 10.4 to 6.8 mm. According to the comparison with local meteorological data from the closest

418 weather station, these two classified intensities can be termed as moderate rainfall intensity events
419 and high-intensity storm events respectively. Both of which can produce surface runoff on local
420 slopes in the study area. In our simulation experiments, the rainfall intensity shows a positive
421 relationship with the depth of surface runoff under all vegetation covers. The high rainfall intensity
422 occurring in short duration results in a higher runoff depth (Krisnayanti et al., 2021). The diameter
423 and threshold raindrop velocity tends to increase with higher intensity rainfall. This event is
424 particularly noticeable when the rainfall intensity is at level 4. Heavy raindrops provide more
425 kinetic energy which changes the surface roughness producing pores blockage and soil crusts,
426 which yield higher surface runoff (Lu et al., 2016).

427 The increasing surface runoff depth is positively related to rainfall intensity at the same slope
428 inclination level and displayed order of $2.5 \text{ mm min}^{-1} < 2.7\text{-}3.3 \text{ mm min}^{-1} < 3.4\text{-}4 \text{ mm min}^{-1} < 4 \text{ mm}$
429 min^{-1} (Fig. 5B). However, the analyses of the relationship between slope gradient and runoff show
430 increasing surface runoff were observed when the slope increased from 1–3 % (level 2) to >5%
431 (level4) with runoff depth of 10.66 mm and 15.93 mm, respectively. However, it was decreased
432 from 13.573 mm to 10.66 mm despite an increasing slope gradient from <1 % (level 1) to 3 %
433 (level2) and also dropped to 15.08 mm when the slope was >5 % (level 4). The main reason is that
434 observations at slope levels 1 and 2 are performed for soil class 1 and class 2, with high and
435 moderate permeability, respectively (Fig. 2A). Previous studies also indicate that surface flow
436 decreases with increasing slope gradient as the rain-bearing area becomes small as at smaller slope
437 gradient the infiltration time is longer at the beginning with high permeable soil conditions (Deng
438 et al., 2019; Wu et al., 2018a). Also, other studies show that surface runoff increases and tend to
439 stabilize with the further increase of the slope gradient (Zhong and Zhang, 2011) but some studies
440 also show that runoff increases first and then start decreasing with increasing slope gradient
441 (Jourgholami et al., 2021; Li et al., 2020; Li and Yu, 2012). The present study shows similar results.
442 Guo et al., (2018) showed that runoff depth is directly related to rainfall intensity and in a negative
443 relationship with slope gradient. Infiltration rates decrease as slope increases from 6° to 35° and,
444 thus, runoff depth increases to a certain extent until a critical slope gradient of 11° is reached at
445 which infiltration rate trend starts changing (Liu et al., 2015). With further increments in slope, the
446 runoff depth gradually decreases (Jourgholami et al., 2021; Nassif and Wilson, 1975). The rainfall
447 intensity has more impact on runoff than slope gradient in this study which is in line with the work

448 by (Wu et al., 2018b). Since the slope gradients at our research site are well below 10 degrees the
449 stronger impact of rainfall intensities agrees with other studies (Liu et al., 2015)

450 In this study, vegetation cover had a positive relationship with runoff depth. Fig. 5B shows that
451 from level 1 (1-5 %) to level 2 (0 %) of vegetation cover there is an abrupt increase in surface
452 runoff as on bare soil there are no interception losses. Then the runoff depth increases with
453 increasing vegetation cover from level 3 (10-15 %) to level 4 (>15 %). The runoff depth was in the
454 order of level 4 > level 2 > level 3 > level 1 of vegetation cover for both high and low rainfall
455 intensity and all slope gradients. However, many studies show that runoff decreases with increasing
456 vegetation cover due to higher canopy interception and rain redistribution reduces energy and
457 runoff depth (He et al., 2020; Loch, 2000; Meng et al., 2007; Tong Li et al., 2020). The reason for
458 high runoff depth at high vegetation cover can be hydrophobic repellency (De Jonge et al., 2007;
459 Hermansen et al., 2019; Knadel et al., 2016) of the surface soil, as higher vegetation cover extracts
460 more soil water. In fact, low soil moisture conditions under higher vegetation cover as noted during
461 the field experiments. Many studies have reported that surface runoff depth increases under dry
462 conditions such as drought periods (Burch et al., 1989; Buttle and Turcotte, 1999; Gomi et al.,
463 2008; Sosa-Pérez and MacDonald, 2017). These studies suggested that the generation of
464 hydrophobic soil surface conditions was one of the main reasons for this phenomenon under dry
465 conditions. (Burch et al., 1989) for example, found that runoff depth increases from 5 % to 15 %
466 due to the hydrophobic conditions after drought or dry summer. These previous studies suggest
467 that because of drought development water repellent soil surface conditions produce more surface
468 runoff regardless of high vegetation cover. The size of the plot can also have a significant impact
469 on the runoff depth. Results obtained by Smets et al. (2008) indicate that there is significant
470 variation in the effectiveness of vegetation cover on runoff if the plot is less than 11m long. Plot
471 scale significantly affects the influence of surface roughness and vegetation cover on sediment
472 yield and runoff depth (Jourgholami and Labelle, 2020).

473 The runoff depth changed with changing silt and organic material content among plots and results
474 suggest that effects are significant ($p < 0.027$). The results agree with Vaezi et al. (2010), who also
475 observed that runoff significantly correlated with silt ($p < 0.001$) and organic material ($p < 0.05$).
476 Organic material positively affects the soil permeability, hence reducing the surface runoff depth
477 (Sepaskhah and Bazrafshan-Jahromi, 2006). A similar pattern was observed for levels 1, 2, and 4
478 of this factor with the runoff averaging 14.05 mm, 13.82 mm, and 12.50 mm, respectively. Slightly

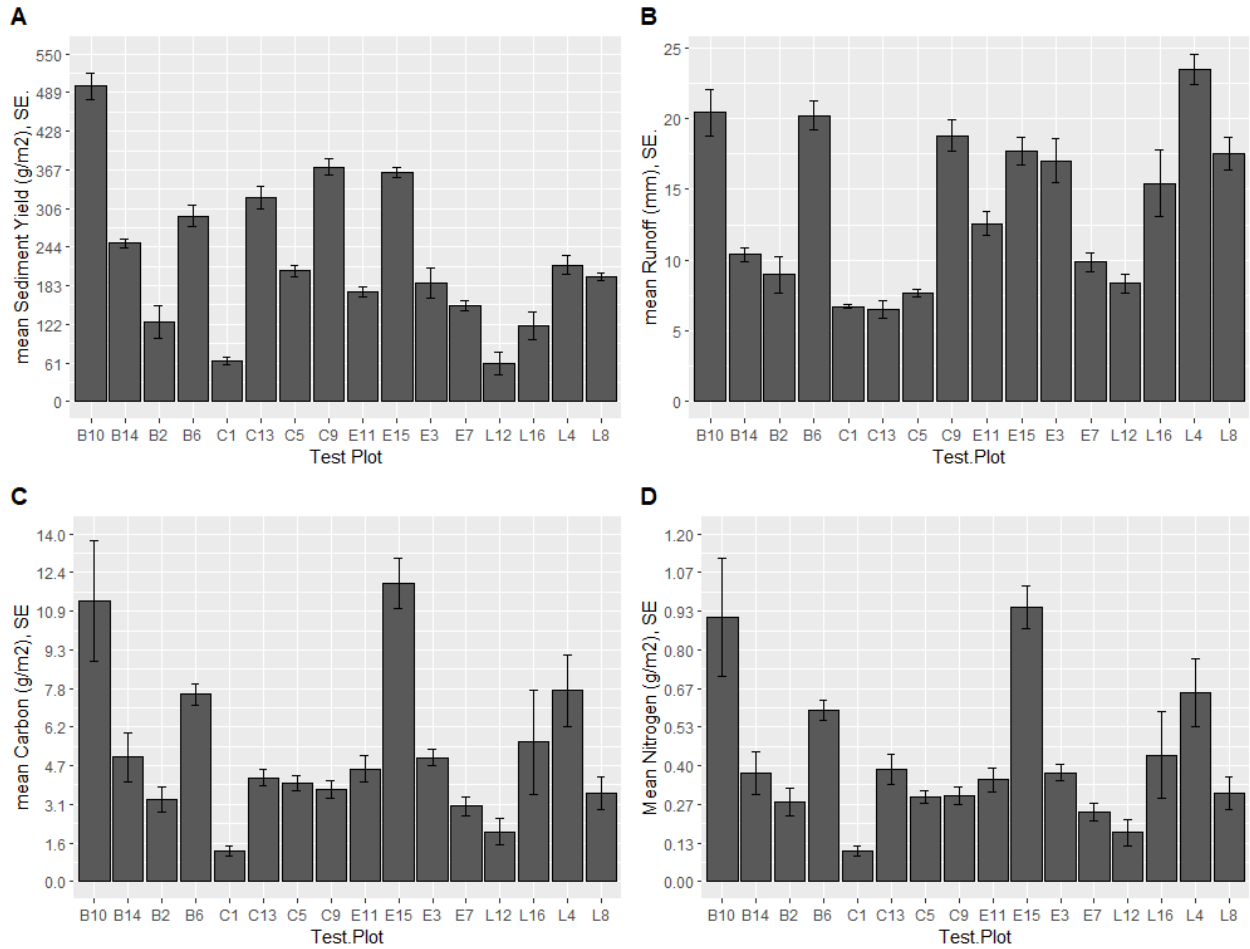
479 increasing runoff depth at level 3 was observed. Results agree with studies indicating that the
480 primary factors affecting surface runoff during rainfall simulation experiments are current soil
481 moisture levels, soil texture, slope, and rainfall intensity (Wang et al., 2016; Ziadat and Taimeh,
482 2013b). The highest runoff was recorded with 23 mm at plot B10 where SiltOM was at level 3 (Fig.
483 4) (Table. 4) and depth to loamy layer < 40 cm (Fig. 2). Later the runoff depth tends to decrease
484 to 12.4 mm as SiltOM percentage increases in the field to level 4. A general trend in this study
485 depicts that with increasing SiltOM content there is a decrease in surface runoff depth with a slight
486 difference at level 3 The depth to a loamy layer (DLL) may act contrary to the effect of the silt
487 content on runoff depth. A thicker sandy topsoil (i.e. deeper depth to loamy layer) may positively
488 affect the soil permeability increasing the infiltration and consequently reducing the surface runoff
489 depth. Thus, spatial variation in these soil properties in the study area noticeably influences the
490 runoff generation in the test plots. This has been also proved in previous studies (Brakensiek and
491 Rawls, 1994; Hrabovský et al., 2020; Meena et al., 2020) mentioning that spatial variability of
492 infiltration capacity is related to the spatial variability of topsoil characteristics that consequently
493 affect the runoff generation.

494 3.3. Carbon and Nitrogen concentration in sediment yield

495 Soil carbon and nitrogen concentration redistribution is strongly governed by the amount of
496 detached sediment within cultivated lands and it is generally accepted that C and N are
497 preferentially transported during soil erosion (Holz and Augustin, 2021). The average values of
498 carbon and nitrogen losses under each level of vegetation cover, slope, and rainfall intensities are
499 presented in Fig. 4C & 4D respectively. Nitrogen and carbon contents of observed sediment yields
500 are highly correlated and vary among experimental plots (Fig 4. C & D). Total C and N losses
501 ranged between 12 ± 1.02 to 3.29 ± 0.496 g m⁻² and 0.948 ± 0.073 to 0.106 ± 0.016 g m⁻² respectively
502 with moderate to high standard deviation, depending on RI, vegetation cover percentage, and
503 SiltOM content (Fig. 4. C & D). As reported for the soil loss, C and N losses on the plots were
504 positively related to the rainfall intensity ranging between 2.8 to 7.7 g m⁻² and 0.2 to 0.4 g m⁻² (Fig.
505 4).

506 In Figure 5C and 5D, it is obvious that the highest nutrient losses were found at vegetation cover
507 more than 0 % despite other land covers percentages contributing less to the nutrient losses (Fig.
508 5. C & D). However, C and N losses were higher in at a vegetation cover of 15 % and in barren

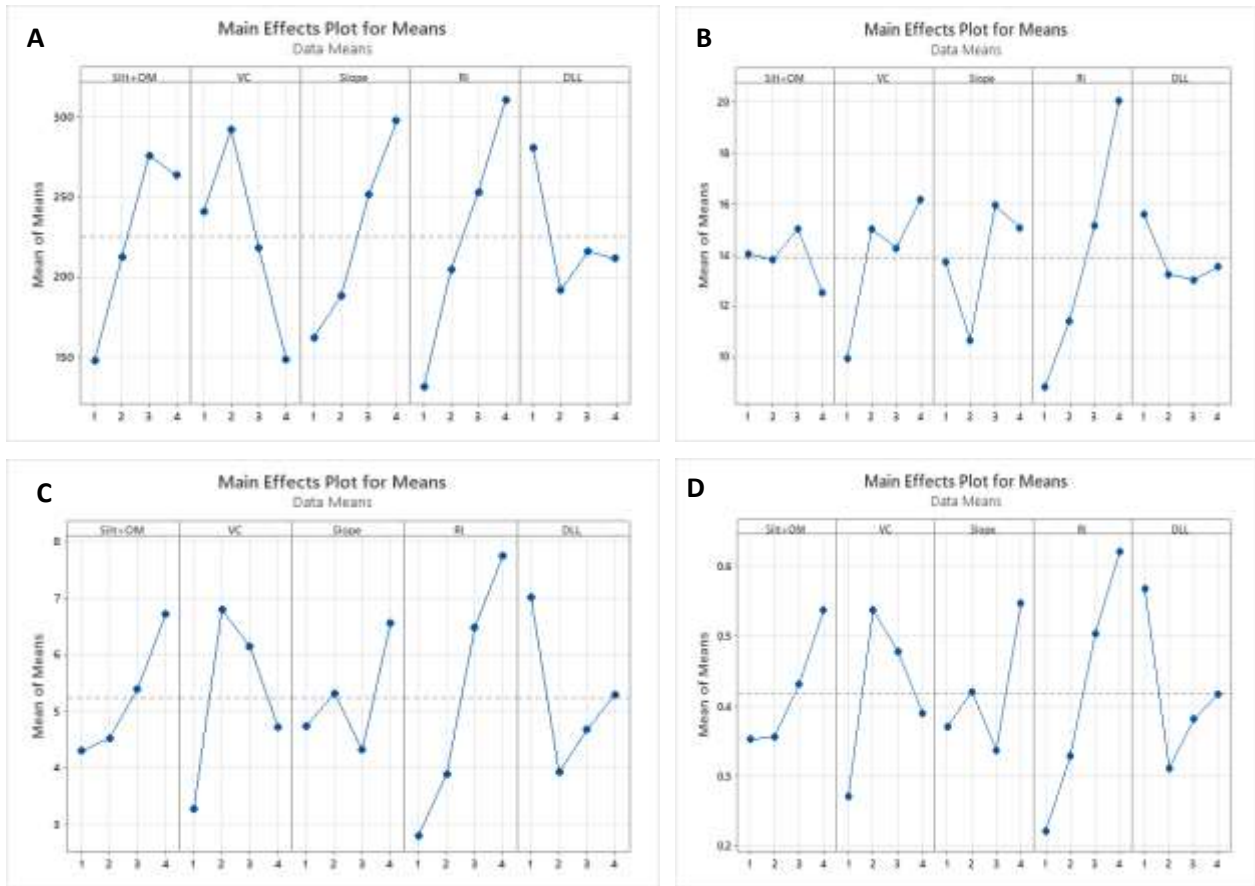
509 land when the soil was subjected to rainfall intensity level 4 (4 mm min^{-1}) (Fig. 4. C & D). This
510 behavior is related to the absence of topsoil protective cover that reduces the impact of raindrops
511 and detachment of soil particles (Nunes et al., 2011). The highest C loss was found under RI of $>$
512 4 mm min^{-1} with values ranging between $12 \pm 1.02 \text{ g m}^{-2}$ and $7.68 \pm 1.12 \text{ g m}^{-2}$ after 8 min rainfall,
513 respectively for vegetation cover levels 4 and 3 (Fig. 5C). Regarding N losses, the highest losses
514 were recorded in the plots with the highest C losses. The smallest C and N loss was observed as
515 2.8 and 0.2 g m^{-2} respectively at low rainfall intensities when detachment forces were small (Fig.
516 5. C & D). The experiments carried out in this study confirm the soil susceptibility to loose nutrients
517 under specific vegetation cover, even at a low rainfall intensity level ($< 2.5 \text{ mm min}^{-1}$). All the
518 study plots have varying silt and organic matter contents, which made soils to lose nutrients
519 defining crusting indexes (Awadhwal and Thierstein, 1985). The different values of runoff induce
520 differences in sediment yield and transport of nutrients. Higher rainfall intensities produce higher
521 runoff depth. It could be confirmed that nutrient losses increase exponentially with higher rainfall
522 intensities. The analysis of slope gradient effect on nutrient loss, where higher soil losses occur,
523 shows that soil sealing can be the main factor that limits runoff as it does not increase significantly
524 with increasing slope (Fig. 5B) (Ramos et al., 2019). However, as sediment yields are increasing
525 with an increasing slope so do the C and N losses captured in the collected sediments except at
526 slope level 3 where C and N losses are reduced as slope increases from level 2 to level 3. The
527 reason is probably that the plots with slope level 3 lie in soil class 3 with throughout sandy texture
528 and lower C and N concentrations in the topsoil (Yost and Hartemink, 2019). The results suggest
529 that a permanent vegetation cover is essential to reduce C and N losses.



530
 531 **Fig. 4: Mean temporal variations and standard error (SE) in sediment yield, runoff, carbon,**
 532 **and nitrogen in relation to heterogeneous field conditions**

533
 534 **Table 3: Mean sediment yield observed under changing soil surface conditions (vegetation**
 535 **cover factor levels)**

Field condition	Vegetation cover	Mean sediment yield	Standard error
	%		
Cultivation	5	241	31.1
Seedbed reparation	0	292	35.8
Emergence stage	10	219	22.5
Leaf development (3 Leaves unfold)	15	149	17.7



538

539 **Fig. 5: Analysis of means (ANOM) for A: Sediment yield (g m⁻²), B: Runoff (mm), C: Carbon**
 540 **(g m⁻²), D: Nitrogen content (g m⁻²). Mean values for each level of each factor (blue dots) and**
 541 **the overall mean of each factor (dashed green line) are shown.**

542 3.4. Optimal conditions for maximum sediment yield, surface runoff, Nitrogen, and Carbon
 543 content

544 The obtained S/N ratio responses for sediment yield, surface runoff, carbon, and nitrogen content
 545 are shown in Table 4 and Table 5. A Higher S/N ratio implies low variations between the desired
 546 output and the measured output. The maximum S/N ratio values among the 16 experiments,
 547 indicated in table 4 were 53.97 for sediment yield and 26.21 for runoff, 21.59 and -0.81 for C and
 548 N losses respectively in the test plot 10 with factor combination of SiltOM₃-VC₂-SS₄-RI₃-DLL₁
 549 (Table 4). Inserting these values from table 4 into Eqn. 2 resulted in mean values of S/N ratios for
 550 each factor level. The maximum values of means of the S/N ratio were then identified. The bold
 551 values in Table 5 show the factor level with the highest S/N ratio for each factor and output variable
 552 (sediment yield, runoff, C and N losses). The highest mean S/N ratio for sediment yield was

553 obtained at factor level 4 for SiltOM, SS, and RI, at level 2 for VC, and level 1 for DLL (Table 5).
554 Thus, we can predict that the highest sediment yield should be obtained with the factor level
555 combination SiltOM₄-VC₂-SS₄-RI₄-DLL₁ (Table 5). On the other hand, the lowest sediment yield
556 should be obtained with the factor combination SiltOM₁-VC₄-SS₁-RI₁-DLL₂. The estimated
557 optimum factor level combination for obtaining the highest surface runoff was found to be
558 SiltOM₃-VC₄-SS₃-RI₄-DLL₁ (Table 5). The highest rainfall intensity (>4 mm min⁻¹) led to the
559 highest volumes of runoff, followed by the factor vegetation cover (maximum values at Level 4)
560 (Table 5). Earlier studies showed that surface runoff depth is sensitive to the plot size and type of
561 vegetation (Herweg and Ludi, 1999; Kort et al., 1998; Zuazo and Pleguezuelo, 2008). The optimum
562 condition for maximum C and N losses were found to be SiltOM₄-VC₂-SS₄-RI₄-DLL₁ and SiltOM₄-
563 VC₂-SS₄-RI₄-DLL₁ respectively (Table 5). The results indicate that rainfall intensity was the main
564 factor that most influenced the sediment yield, runoff, C and N losses in the study area followed
565 by vegetation cover and then slope steepness.

566
567
568
569
570
571
572
573
574
575
576
577
578
579
580
581

582 **Table 4: The S/N ratio of each experiment resulting from a different combination of factors**
 583 **and levels.**

Factors/ Plot	Combination of levels					Silt OM (%)	vegetation cover (%)	Slope steepness (%)	Rainfall intensity (mm min ⁻¹)	Depth to loamy layer (cm)	S/N			
	Silt OM	VC	SS	RI	DLL						Sediment yield	Runoff	C	N
1	1	1	1	1	1	>20	1-5	<1	<2.5	<40	36.08	16.53	1.65	-19.47
2	1	2	2	2	2	>20	0	1-3	2.7-3.3	40-55	41.98	19.05	10.35	-11.20
3	1	3	3	3	3	>20	10-15	3-5	3.4-4	55-70	45.47	24.62	13.96	-8.48
4	1	4	4	4	4	>20	>15	>5	>4	>70	46.70	27.42	17.71	-3.72
5	2	1	2	3	4	18-20	1-5	1-3	3.4-4	>70	46.31	17.70	11.96	-10.69
6	2	2	1	4	3	18-20	0	<1	>4	55-70	49.35	26.12	17.55	-4.56
7	2	3	4	1	2	18-20	10-15	>5	<2.5	40-55	43.60	19.87	9.65	-12.44
8	2	4	3	2	1	18-20	>15	3-5	2.7-3.3	<40	45.95	24.87	11.01	-10.35
9	3	1	3	4	2	16-18	1-5	3-5	>4	40-55	51.39	25.48	11.43	-10.58
10	3	2	4	3	1	16-18	0	>5	3.4-4	<40	53.97	26.21	21.59	-0.81
11	3	3	1	2	4	16-18	10-15	<1	2.7-3.3	>70	44.75	21.98	13.13	-9.09
12	3	4	2	1	3	16-18	>15	1-3	<2.5	55-70	35.63	18.42	6.02	-15.45
13	4	1	4	2	3	<16	1-5	>5	2.7-3.3	55-70	50.18	16.31	12.41	-8.20
14	4	2	3	1	4	<16	0	3-5	<2.5	>70	47.97	20.32	13.99	-8.54
15	4	3	2	4	1	<16	10-15	1-3	>4	<40	51.18	24.95	21.05	-0.46
16	4	4	1	3	2	<16	>15	<1	3.4-4	40-55	41.52	23.76	15.01	-7.19

584

585

586

587

588

589

590

591

592

593

594 **Table 5: Mean S/N ratio response table for the investigated experimental factors**

Output Parameter	Experimental factors	Mean S/N ratio				Delta	Rank
		Level 1	Level 2	Level 3	Level 4		
Sediment Yield	Silt+Organic material	42.56	46.30	46.44	47.71	5.15	4
	Vegetation Cover	45.99	48.32	46.25	42.45	5.87	2
	Slope Steepness	42.92	43.78	47.69	48.61	5.69	3
	Rainfall Intensity	40.82	45.71	46.82	49.65	8.83	1
	Depth to Loamy Layer	46.79	44.62	45.16	46.43	2.17	5
Runoff	Silt+ Organic material	21.91	22.14	23.02	21.34	1.69	5
	Vegetation Cover	19.01	22.93	22.86	23.62	4.61	2
	Slope Steepness	22.1	20.03	23.82	22.45	3.79	3
	Rainfall Intensity	18.79	20.56	23.07	25.99	7.21	1
	Depth to Loamy Layer	23.14	22.04	21.37	21.86	1.78	4
Carbon	Silt+ Organic material	10.92	12.54	12.91	15.75	4.83	3
	Vegetation Cover	9.36	15.74	14.58	12.44	6.37	2
	Slope Steepness	11.83	12.48	12.60	15.21	3.37	4
	Rainfall Intensity	7.83	11.73	15.50	17.07	9.24	1
	Depth to Loamy Layer	13.83	11.61	12.49	14.20	2.59	5
Nitrogen	Silt+ Organic material	-10.72	-9.51	-8.98	-6.10	4.61	3
	Vegetation Cover	-12.24	-6.28	-7.62	-9.18	5.95	2
	Slope Steepness	-10.08	-9.45	-9.49	-6.29	3.78	4
	Rainfall Intensity	-13.97	-9.71	-6.79	-4.83	9.14	1
	Depth to Loamy Layer	-7.77	-10.35	-9.17	-8.01	2.58	5

595

596 3.5. Percentage contribution of the experimental factors to sediment yield, runoff, C and N

597 losses

598 ANOVA was used to estimate the contribution of the individual factors to sediment yield, runoff,

599 C and N losses (Table 6). Rainfall intensity contributed most strongly to sediment yield (40.55 %)

600 followed by slope steepness (23.76 %) and vegetation cover (17.73 %). (Peng and Wang, 2012)

601 indicated that soil loss is positively related to rainfall events with high antecedent precipitations.

602 The slope gradient can be more important than vegetation cover because of its relation with the

603 underlying geological formations resulting in varying soil characteristics. In consequence, slope
604 gradients are related to soil moisture and hence the soil's susceptibility to soil detachment.
605 Vegetation cover yields higher soil moisture at low to moderate slopes but it falls sharply at steeper
606 slopes as soil permeability decreases that increases runoff till a threshold slope, moreover, the flow
607 velocity becomes larger with increasing slope gradient due to increasing shear stress (Defersha and
608 Melesse, 2012). The impact duration of runoff on steeper slopes becomes smaller and hence it
609 weakens the protecting effect of surface seal, increasing the impact of rainfall splashing on the soil
610 surface (Zhao et al., 2015). It produces more detachment of soil particles and transportation.
611 However, the sum of silt content and organic material only contributes 14.77 % to sediment yield.
612 (Ziadat and Taimeh, 2013a) showed a significant correlation between the ultimate infiltration rate
613 and soil properties such as organic matter ($R = 0.48$) and silt content ($R = 0.72$). The low
614 contribution of silt and organic matter to our results is most likely related to their comparatively
615 low variation among measurement plots and due to the high content of organic matter that is
616 varying from 2.3 to 2.4 % among the test plots. The high organic matter improves the aggregate
617 stability, reduces the bulk density, and increases moisture retention and soil shear strength that
618 helps in soil stability and resistance against erosion (Ekwue, 1990). Previous studies also concluded
619 that aggregate stability is closely and negatively related to the soil detachment from field
620 experiments under rainfall simulators on micro plots (Roth et al., 1987; Van Dijk et al., 1996). The
621 factor of least importance in our study was the depth to the loamy layer (DLL) (3.17 %). This can
622 be explained by the fact that the loamy layer with low permeability generally starts at relatively
623 deep depths (lowest depth approximately 38 cm) and at many locations sand-filled pre-glacial ice
624 cracks with higher permeability were observed in the loamy layer (Kühn, 2003). Therefore,
625 differences in permeability and water storage capacity (risk of waterlogged soils) between
626 experimental plots were probably relatively low. ANOVA results for the nitrogen (N) and carbon
627 (C) content of sediment yield were similar (Table 6). As for sediment yield, rainfall intensity
628 contributed most to the overall variation of C and N contents. The respective percentage
629 contribution of rainfall intensity, vegetation cover, SiltOM content, slope and depth to loamy layer
630 was 51.70%, 21.50 %, 12.55 %, 9.63 % and 4.62 % respectively for Nitrogen content and 52.31
631 %, 24.07 %, 12.39 %, 6.81 % and 4.41 % respectively for Carbon content. Runoff was mostly
632 influenced by rainfall intensity (55.45 %) followed by vegetation cover, slope, depth to loamy
633 layer, and SiltOM content. The respective contribution was 55.45 %, 24.71 %, 3.18 %, and 2.78 %
634 (Table 6), agreeing with the findings of (Kirkby et al., 2004). The stronger impact of vegetation

635 cover compared with the slope can be explained by the stronger variability of vegetation cover at
 636 different soil management stages during the experimental period in the study area. In addition, at
 637 different slope levels varying soil compositions and moisture content affect the potential of surface
 638 runoff.

639 **Table 6: Percentage contribution of each factor (ρ_F %) for the different output parameters**
 640 **as estimated by ANOVA**

Output Parameters	ρ_F %				
	SiltOM	Vegetation cover	Slope steepness	Rainfall intensity	Depth to Loamy Layer
Sediment yield	14.77	17.74	23.77	40.56	3.17
Runoff	2.78	24.71	13.88	55.45	3.18
Nitrogen content	12.55	21.50	9.63	51.70	4.62
Carbon content	12.39	24.07	6.81	52.31	4.41

641

642

673 3.6.Linear regression models

674 Linear regression models are used to predict sediment yield, runoff, as well as C and N losses as a
 675 function of Silt + OM, vegetation cover, slope, rainfall intensity, and depth to the loamy layer. No
 676 transformation has been performed on the response variables. The estimated regression models are
 677 shown in the Eqns. (8-11).

678 Sediment yield = -7.2 + 40.9 SiltOM - 35.1 VC + 46.9 Slope + 58.6 RI - 18.4 DLL

679 ($R^2 = 82.53$) (8)

680 Runoff = 0.10 - 0.341 SiltOM + 1.807 VC + 0.933 Slope + 3.743 RI - 0.641 DLL

681 ($R^2 = 79.66$) (9)

682 C = -2.08 + 0.810 SiltOM + 0.371 VC + 0.446 Slope + 1.736 RI - 0.440 DLL

683 ($R^2 = 60.97$) (10)

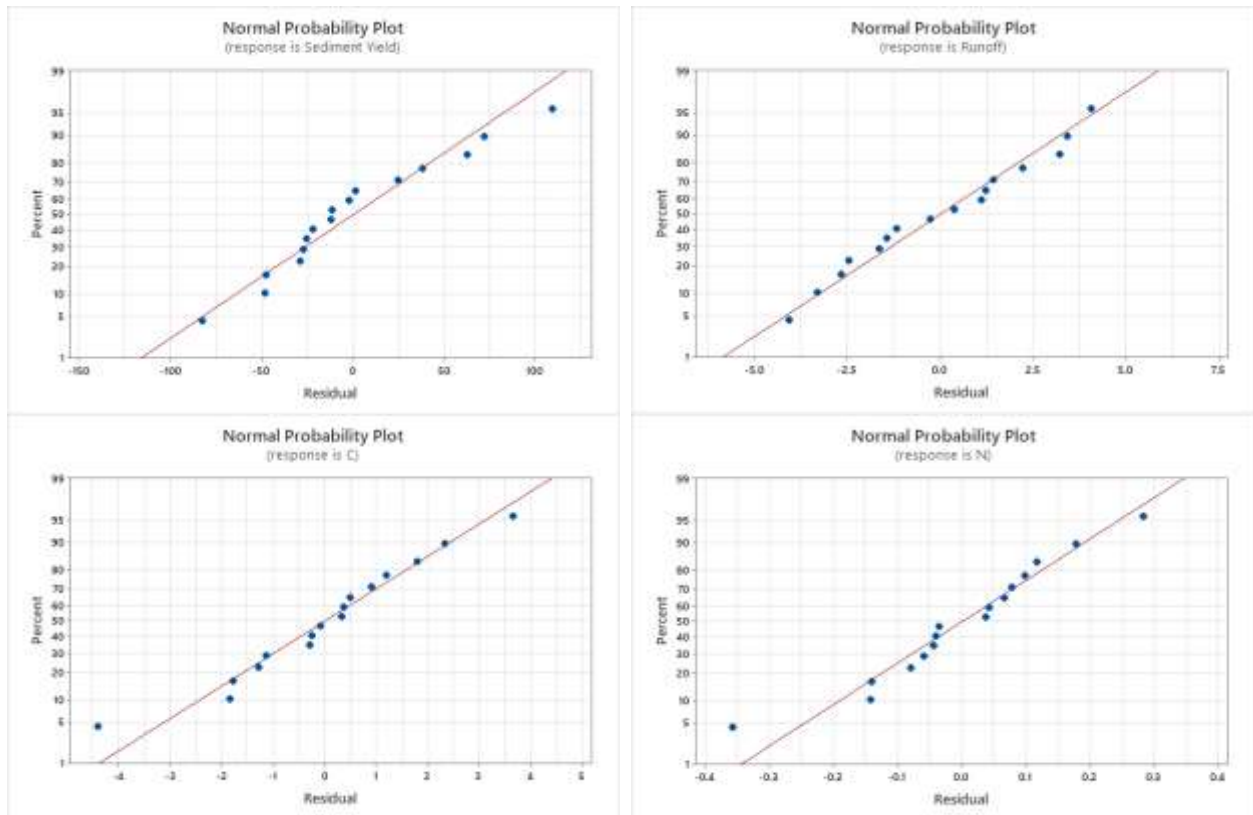
684 N = -0.172 + 0.0629 SiltOM + 0.0299 VC + 0.0445 Slope + 0.1373 RI - 0.0381 DLL

685 ($R^2 = 62.13$) (11)

686 Where sediment yield, runoff depth, C and N are $g\ m^{-2}$, SiltOM and VC are %.

687

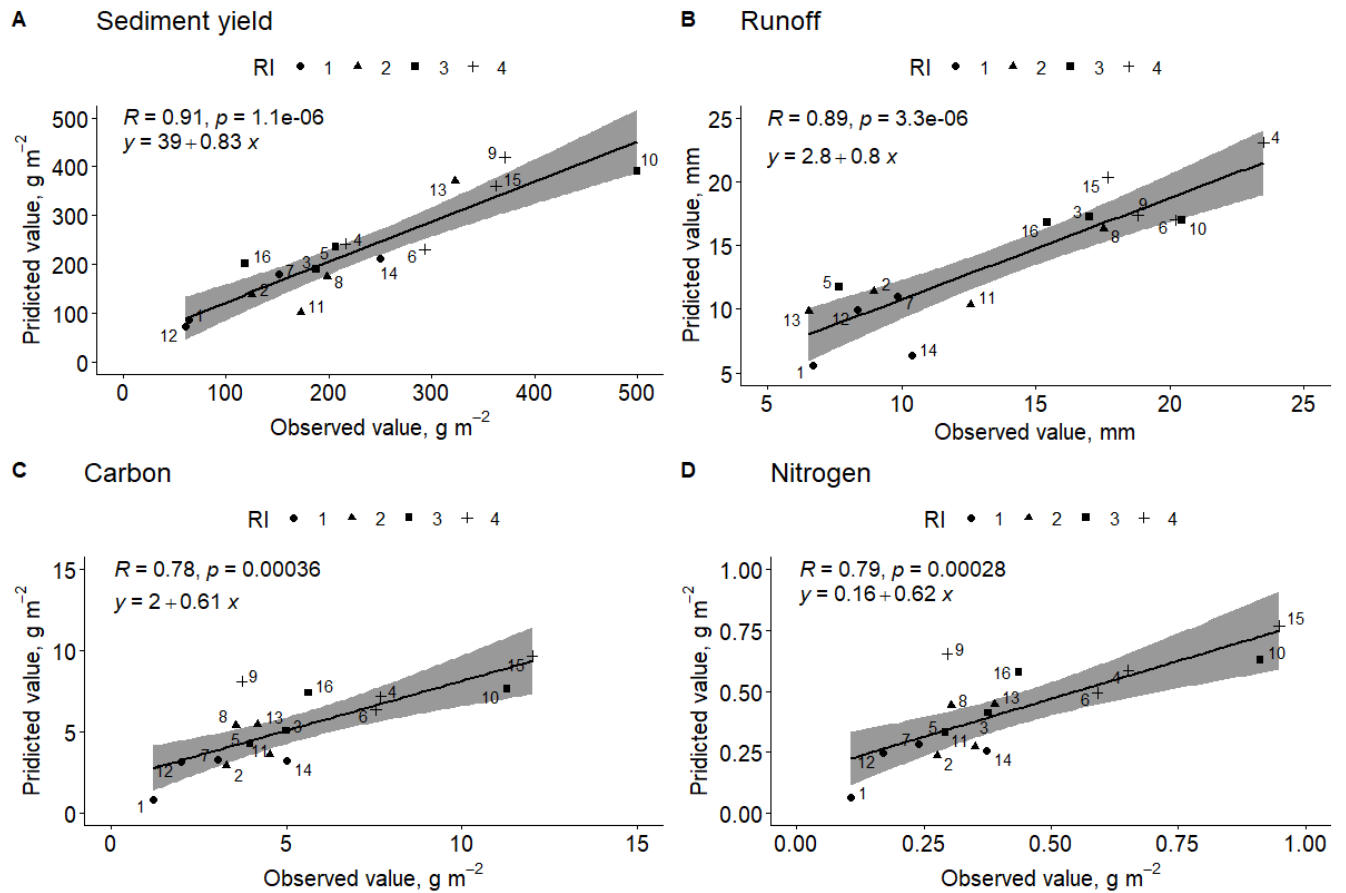
688 The capability of these empirical regression models was checked by using the coefficient of
689 determination R^2 . Regression models for sediment yield, runoff, carbon, and nitrogen yielded R^2
690 values of 82.53 %, 79.66 %, 60.97 %, and 62.13 % respectively. Residual plots (Fig. 7 A, B, C &
691 D) indicate that residuals are independent and normally distributed. Sediment yield is positively
692 related to SiltOM but runoff depth is negatively related. This indicates that a high amount of SiltOM
693 would increase the erodibility of the soil but would reduce the runoff rate. This is also evident from
694 Fig. 5A and B. The sediment yield is more sensitive to SiltOM compared to runoff. Coefficients of
695 SiltOM for C and N losses show a positive relationship. C was more responsive to SiltOM as
696 compared to N. It is suggested to have further research to find a threshold point for SiltOM in the
697 soil to achieve the lowest sediment yield and runoff. Fig. 8 represents the scatter plot of predicted
698 vs observed values with high R^2 . The shaded band is a pointwise 95 % confidence interval on the
699 fitted values. These results confirm the ability of the Taguchi method for the prediction of soil
700 erosion in response to different combinations of factors/levels. The regression equation for
701 sediment yield was further applied to predict sediment yields across the entire field for identifying
702 areas within the field that have a higher susceptibility to soil erosion (Fig. 9).



703

704 **Fig. 7: Distribution of residuals of the regression models for sediment yield, runoff, carbon,**
 705 **and nitrogen**

706



707

708

709 **Fig. 8: Predicted versus observed sediment yield, runoff depth, carbon, and nitrogen losses**

710

711

712

713

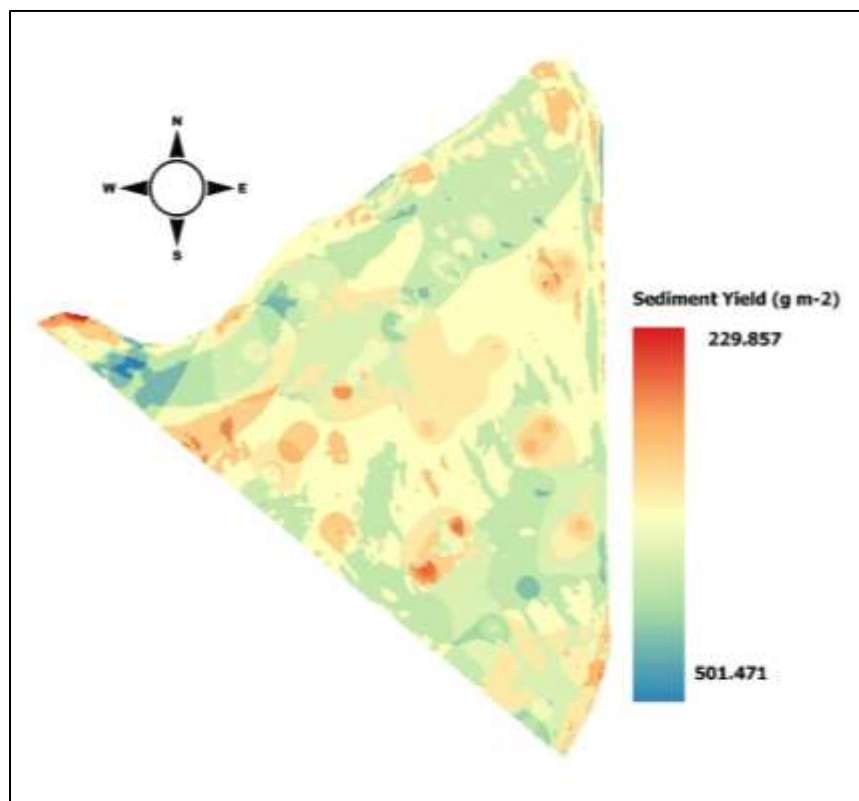
714

715

716

717

718



719

720

721 **Fig. 9: Identification of potential soil erosion risk areas**

722 **4. Conclusion**

723 Different scenarios were tested with 16 effective simulated rainfall events under different rainfall
 724 intensities, vegetation cover, heterogeneous in-field slope, and soil conditions. The results
 725 indicated that runoff, soil, and CN losses increase with increasing rainfall intensity. It was observed
 726 that sediment yield, overland flow, CN content were greatly affected by rainfall intensity having a
 727 contribution of 40.56 %, 55.45 %, 51.70 %, and 52.31 % respectively among the other factors.
 728 However, the least contributing factor was depth to loamy layer for all output variables except for
 729 surface runoff. The results show that the worst conditions among 16 plots were at SiltOM₃-VC₂-
 730 SS₄-RI₃-DLL₁ for sediment yield. However, predicted experimental factors for the highest
 731 sediment yield were found with the factor combination SiltOM₄-VC₂-SS₄-RI₄-DLL₁ and the lowest
 732 sediment yield was observed with the factor combination SiltOM₁-VC₄-SS₁-RI₁-DLL₂. The
 733 threshold rainfall intensity for soil erosion was 2.5 mm min⁻¹. VC and DLL are inversely correlated
 734 with sediment yield, while SiltOM, slope, and rainfall intensity are directly correlated.

735 The surface runoff was negatively related to SiltOM and DLL, but the vegetative cover, slope, and
 736 rainfall intensity positively affect the runoff. Regarding, C and N, except the DLL, other factors
 737 show a positive correlation. Based on the experimental results, statistical regression models were
 738 developed, which were applied for identifying the erosion risk areas at the field scale. The applied
 739 workflow allowed for efficiently predicting soil erosion and identifying areas susceptible to soil
 740 loss at a high spatial resolution. The study approved the capabilities of Taguchi's fractional

741 factorial design to efficiently analyze the response of soil erosion to dominant driving factors and
742 detect and quantify in-field heterogeneity of erosion risk areas. The statistical models generated in
743 this study can be used by environmental agencies and farmers for spatially explicit application of
744 erosion control measures within fields with high spatial heterogeneity. Further, it is suggested that
745 combining GIS with such numerical models can give great benefits for water quality control and
746 soil management on larger scales with intensive spatial heterogeneous field conditions.

747 **CRedit authorship contribution statement**

748 Conceptualization, A.R., T.G., M.H.R., and H.A.; methodology, A.R., M.H.R., T.G., and H.A.; re-
749 source and data curation, A.R., T.G., and H.A., writing-original draft preparation, A.R.; writing-
750 review and editing, T.G., M.H.R., H.A., and A.R.; visualization, M.H.R., H.A., and T.G.;
751 supervision, T.G.; project administration, T.G.; funding acquisition, T.G., H.A.; All authors have
752 read and agreed to the published version of the manuscript.

753 **Funding**

754 This research was funded by the German Federal Ministry of Education and Research (BMBF)
755 through the Digital Agriculture Knowledge and Information System (DAKIS) Project, grant
756 number 031B0729E, and by the Deutsche Forschungsgemeinschaft (DFG, German Research
757 Foundation) under Germany's Excellence Strategy-EXC 2070-390732324 (PhenoRob). The APC
758 was funded by the Crop Science Group, University of Bonn, Germany.

759 **Declaration of competing interest**

760 The authors declare that they have no known competing financial interests or personal relationships
761 that could have appeared to influence the work reported in this paper.

762 **References**

- 763 Aga, A.O., Melesse, A.M., Chane, B., 2020. An alternative empirical model to estimate
764 watershed sediment yield based on hydrology and geomorphology of the basin in data-
765 scarce rift VALLEY lake regions, Ethiopia. *Geosci.* 10.
766 <https://doi.org/10.3390/geosciences10010031>
- 767 Albaladejo Montoro, J., Stocking, M., 1989. Comparative evaluation of two models in predicting
768 storm soil loss from erosion plots in semi-arid Spain. *Catena* 16, 227–236.
769 [https://doi.org/10.1016/0341-8162\(89\)90010-6](https://doi.org/10.1016/0341-8162(89)90010-6)
- 770 Anh, P.T.Q., Gomi, T., MacDonald, L.H., Mizugaki, S., Van Khoa, P., Furuichi, T., 2014.
771 Linkages among land use, macronutrient levels, and soil erosion in northern Vietnam: A
772 plot-scale study. *Geoderma* 232–234, 352–362.
773 <https://doi.org/10.1016/j.geoderma.2014.05.011>
- 774 Awadhwai, N.K., Thierstein, G.E., 1985. Soil crust and its impact on crop establishment: A
775 review. *Soil Tillage Res.* 5, 289–302. [https://doi.org/10.1016/0167-1987\(85\)90021-2](https://doi.org/10.1016/0167-1987(85)90021-2)
- 776 Barthès, B., Roose, E., 2002. Aggregate stability as an indicator of soil susceptibility to runoff
777 and erosion; validation at several levels. *Catena* 47, 133–149. [https://doi.org/10.1016/S0341-8162\(01\)00180-1](https://doi.org/10.1016/S0341-8162(01)00180-1)
778

- 779 Baruah, S., Ramalingam, K., Kannan, B., Kaliaperumal, R., 2019. Soil erodibility estimation and
780 its correlation with soil properties in Coimbatore district Soil erodibility estimation and its
781 correlation with soil properties in Coimbatore district. *Int. J. Chem. Stud.* 7, 3327–3332.
- 782 Benjeddou, O., Soussi, C., Jedidi, M., Benali, M., 2017. Experimental and theoretical study of the
783 effect of the particle size of limestone fillers on the rheology of self-compacting concrete. *J.*
784 *Build. Eng.* 10, 32–41. <https://doi.org/10.1016/J.JOBE.2017.02.003>
- 785 Brakensiek, D.L., Rawls, W.J., 1994. Soil containing rock fragments: effects on infiltration.
786 *CATENA* 23, 99–110. [https://doi.org/10.1016/0341-8162\(94\)90056-6](https://doi.org/10.1016/0341-8162(94)90056-6)
- 787 Burch, G.J., Moore, I.D., Burns, J., 1989. Soil hydrophobic effects on infiltration and catchment
788 runoff. *Hydrol. Process.* 3, 211–222. <https://doi.org/10.1002/HYP.3360030302>
- 789 Buttle, J.M., Turcotte, D.S., 1999. Runoff processes on a forested slope on the Canadian shield.
790 *Nord. Hydrol.* 30, 1–20. <https://doi.org/10.2166/nh.1999.0001>
- 791 Cerdà, A., Lucas-Borja, M.E., Franch-Pardo, I., Úbeda, X., Novara, A., López-Vicente, M.,
792 Popović, Z., Pulido, M., 2021. The role of plant species on runoff and soil erosion in a
793 Mediterranean shrubland. *Sci. Total Environ.* 799, 149218.
794 <https://doi.org/10.1016/j.scitotenv.2021.149218>
- 795 Cerdan, O., Govers, G., Le Bissonnais, Y., Van Oost, K., Poesen, J., Saby, N., Gobin, A., Vacca,
796 A., Quinton, J., Auerswald, K., Klik, A., Kwaad, F.J.P.M., Raclot, D., Ionita, I., Rejman, J.,
797 Rousseva, S., Muxart, T., Roxo, M.J., Dostal, T., 2010. Rates and spatial variations of soil
798 erosion in Europe: A study based on erosion plot data. *Geomorphology* 122, 167–177.
799 <https://doi.org/10.1016/j.geomorph.2010.06.011>
- 800 Chmelová, R., Šarapatka, B., 2002. Soil erosion by water: Contemporary research methods and
801 their use. *Geographica* 37, 23–30.
- 802 Chou, C.S., Yang, R.Y., Chen, J.H., Chou, S.W., 2010. The optimum conditions for preparing the
803 lead-free piezoelectric ceramic of Bi_{0.5}Na_{0.5}TiO₃ using the Taguchi method. *Powder*
804 *Technol.* 199, 264–271. <https://doi.org/10.1016/j.powtec.2010.01.015>
- 805 Cox, N.J., Warburton, J., Armstrong, A., Holliday, V.J., 2008. Fitting concentration and load
806 rating curves with generalized linear models. *Earth Surf. Process. Landforms* 33, 25–39.
807 <https://doi.org/10.1002/ESP.1523>
- 808 De Jonge, L.W., Moldrup, P., Jacobsen, O.H., 2007. Soil-water content dependency of water
809 repellency in soils. *Soil Sci.* 172, 577–588. <https://doi.org/10.1097/SS.0B013E318065C090>
- 810 Defersha, M.B., Melesse, A.M., 2012. Effect of rainfall intensity, slope and antecedent moisture
811 content on sediment concentration and sediment enrichment ratio. *Catena* 90, 47–52.
812 <https://doi.org/10.1016/j.catena.2011.11.002>
- 813 Deng, L., Zhang, L., Fan, X., Sun, T., Fei, K., Ni, L., 2019. Effects of rainfall intensity and slope
814 gradient on runoff and sediment yield from hillslopes with weathered granite. *Environ. Sci.*
815 *Pollut. Res.* 26, 32559–32573. <https://doi.org/10.1007/s11356-019-06486-z>
- 816 Donjadee, S., Chinnarasri, C., 2012. Effects of rainfall intensity and slope gradient on the
817 application of vetiver grass mulch in soil and water conservation. *Int. J. Sediment Res.* 27,
818 168–177. [https://doi.org/10.1016/S1001-6279\(12\)60025-0](https://doi.org/10.1016/S1001-6279(12)60025-0)

- 819 Duiker, S.W., Flanagan, D.C., Lal, R., 2001. Erodibility and infiltration characteristics of five
820 major soils of southwest Spain. *Catena* 45, 103–121. <https://doi.org/10.1016/S0341->
821 8162(01)00145-X
- 822 Dunj6, G., Pardini, G., Gispert, M., 2004. The role of land use-land cover on runoff generation
823 and sediment yield at a microplot scale, in a small Mediterranean catchment. *J. Arid*
824 *Environ.* 57, 239–256. [https://doi.org/10.1016/S0140-1963\(03\)00097-1](https://doi.org/10.1016/S0140-1963(03)00097-1)
- 825 Ekwue, E.I., 1990. Organic-matter effects on soil strength properties. *Soil Tillage Res.* 16, 289–
826 297. [https://doi.org/10.1016/0167-1987\(90\)90102-J](https://doi.org/10.1016/0167-1987(90)90102-J)
- 827 Eslamian, S., 2014. Handbook of engineering hydrology: Modeling, climate change, and
828 variability. *Handb. Eng. Hydrol. Model. Clim. Chang. Var.* 1–615.
829 <https://doi.org/10.1201/b16683>
- 830 Fern6ndez-G6lvez, J., Barahona, E., Mingorance, M.D., 2008. Measurement of infiltration in
831 small field plots by a portable rainfall simulator: Application to trace-element mobility.
832 *Water. Air. Soil Pollut.* 191, 257–264. <https://doi.org/10.1007/s11270-008-9622-2>
- 833 Gomi, T., Sidle, R.C., Ueno, M., Miyata, S., Kosugi, K., 2008. Characteristics of overland flow
834 generation on steep forested hillslopes of central Japan. *J. Hydrol.* 361, 275–290.
835 <https://doi.org/10.1016/J.JHYDROL.2008.07.045>
- 836 Grismer, M.E., 2012. Mod6lisation de l'6rosion pour la gestion des terres dans le bassin du lac
837 Tahoe, Etats-Unis: scalance depuis les parcelles jusqu'aux bassins versants forestiers.
838 *Hydrol. Sci. J.* 57, 878–900. <https://doi.org/10.1080/02626667.2012.685170>
- 839 Gross, C.M., Angle, J.S., Hill, R.L., Welterlen, M.S., 1991. Runoff and Sediment Losses from
840 Tall Fescue under Simulated Rainfall. *J. Environ. Qual.* 20, 604–607.
841 <https://doi.org/10.2134/jeq1991.00472425002000030017x>
- 842 Guidry, A.R., Schindler, F. V., German, D.R., Gelderman, R.H., Gerwing, J.R., 2006. Using
843 Simulated Rainfall to Evaluate Field and Indoor Surface Runoff Phosphorus Relationships.
844 *J. Environ. Qual.* 35, 2236–2243. <https://doi.org/10.2134/jeq2006.0156>
- 845 Guo, Z., Ma, M., Cai, C., Wu, Y., 2018. Combined effects of simulated rainfall and overland
846 flow on sediment and solute transport in hillslope erosion. *J. Soils Sediments* 18, 1120–
847 1132. <https://doi.org/10.1007/s11368-017-1868-0>
- 848 He, Z., Jia, G., Liu, Z., Zhang, Z., Yu, X., Xiao, P., 2020. Field studies on the influence of
849 rainfall intensity, vegetation cover and slope length on soil moisture infiltration on typical
850 watersheds of the Loess Plateau, China. *Hydrol. Process.* 34, 4904–4919.
851 <https://doi.org/10.1002/hyp.13892>
- 852 Heiskanen, J., 2008. Comparison of three methods for determining the particle density of soil
853 with liquid pycnometers. <http://dx.doi.org/10.1080/00103629209368633> 23, 841–846.
854 <https://doi.org/10.1080/00103629209368633>
- 855 Hermansen, C., Moldrup, P., M6ller, K., Knadel, M., Jonge, L.W. de, 2019. The Relation
856 between Soil Water Repellency and Water Content Can Be Predicted by Vis-NIR
857 Spectroscopy. *Soil Sci. Soc. Am. J.* 83, 1616–1627.
858 <https://doi.org/10.2136/SSSAJ2019.03.0092>

- 859 Herweg, K., Ludi, E., 1999. The performance of selected soil and water conservation measures -
860 Case studies from Ethiopia and Eritrea. *Catena* 36, 99–114. <https://doi.org/10.1016/S0341->
861 8162(99)00004-1
- 862 Holz, M., Augustin, J., 2021. Erosion effects on soil carbon and nitrogen dynamics on cultivated
863 slopes: A meta-analysis. *Geoderma* 397, 115045.
864 <https://doi.org/10.1016/J.GEODERMA.2021.115045>
- 865 Hrabovský, A., Dlapa, P., Cerdà, A., Kollár, J., 2020. The impacts of vineyard afforestation on
866 soil properties, water repellency and near-saturated infiltration in the little carpathians
867 mountains. *Water* 12, 2550. <https://doi.org/10.3390/w12092550>
- 868 Huang, R., Huang, L., He, B., Zhou, L., Wang, F., 2012. Effects of slope forest and grass
869 vegetation on reducing rainfall-runoff erosivity in Three Gorges Reservoir Region. *Nongye*
870 *Gongcheng Xuebao/Transactions Chinese Soc. Agric. Eng.* 28, 70–76.
871 <https://doi.org/10.3969/j.issn.1002-6819.2012.09.012>
- 872 Ihinegbu, C., Ogunwumi, T., 2021. Multi-criteria modelling of drought: a study of Brandenburg
873 Federal State, Germany. *Model. Earth Syst. Environ.* 1, 3. <https://doi.org/10.1007/s40808->
874 021-01197-2
- 875 Issaka, S., Ashraf, M.A., 2017. Impact of soil erosion and degradation on water quality: a review.
876 <https://doi.org/10.1080/24749508.2017.1301053> 1, 1–11.
877 <https://doi.org/10.1080/24749508.2017.1301053>
- 878 J. R. Williams, C. A. Jones, P. T. Dyke, 1984. A Modeling Approach to Determining the
879 Relationship Between Erosion and Soil Productivity. *Trans. ASAE* 27, 0129–0144.
880 <https://doi.org/10.13031/2013.32748>
- 881 Jahun, B.G., Ibrahim, R., Dlamini, N.S., Musa, S.M., 2015. Review of Soil Erosion Assessment
882 using RUSLE Model and GIS. *J. Biol. Agric. Healthc.* 5, 36–47.
- 883 Jebari, S., Berndtsson, R., Bahri, A., Boufaroua, M., 2008. Exceptional Rainfall Characteristics
884 Related to Erosion Risk in Semiarid Tunisia. *Open Hydrol. J.* 2, 25–33.
885 <https://doi.org/10.2174/1874378100802010025>
- 886 Jourgholami, M., Karami, S., Tavankar, F., Lo Monaco, A., Picchio, R., 2021. Effects of slope
887 gradient on runoff and sediment yield on machine-induced compacted soil in temperate
888 forests. *Forests* 12, 1–19. <https://doi.org/10.3390/f12010049>
- 889 Jourgholami, M., Labelle, E.R., 2020. Effects of plot length and soil texture on runoff and
890 sediment yield occurring on machine-trafficked soils in a mixed deciduous forest. *Ann. For.*
891 *Sci.* 77, 1–11. <https://doi.org/10.1007/s13595-020-00938-0>
- 892 Kamphorst, A., 1987. A small rainfall simulator for the determination of soil erodibility.
893 *Netherlands J. Agric. Sci.* 35, 407–415. <https://doi.org/10.18174/NJAS.V35I3.16735>
- 894 Kandel, D.D., Western, A.W., Grayson, R.B., Turrall, H.N., 2004. Process parameterization and
895 temporal scaling in surface runoff and erosion modelling. *Hydrol. Process.* 18, 1423–1446.
896 <https://doi.org/10.1002/hyp.1421>
- 897 Keating, B.A., Carberry, P.S., Hammer, G.L., Probert, M.E., Robertson, M.J., Holzworth, D.,
898 Huth, N.I., Hargreaves, J.N.G., Meinke, H., Hochman, Z., McLean, G., Verburg, K., Snow,

899 V., Dimes, J.P., Silburn, M., Wang, E., Brown, S., Bristow, K.L., Asseng, S., Chapman, S.,
900 McCown, R.L., Freebairn, D.M., Smith, C.J., 2003. An overview of APSIM, a model
901 designed for farming systems simulation. *Eur. J. Agron.* 18, 267–288.
902 [https://doi.org/10.1016/S1161-0301\(02\)00108-9](https://doi.org/10.1016/S1161-0301(02)00108-9)

903 Kirkby, M.J., Jones, R., Irvine, B., Gobin, A., Govers, G., Cerdan, O., Rompaey, A.J.J. Van, Le
904 Bissonnais, Y., Daroussin, J., King, D., Montanarella, L., Grimm, M., Vieillefont, V.,
905 Puigdefabregas, J., Boer, M., Kosmas, C., Yassoglou, N., Tsara, M., Mantel, S., Lynden,
906 G.J. Van, Huting, J., 2004. Pan-European Soil Erosion Risk Assessment: The PESERA
907 Map, Version 1 October 2003. Explanation of Special Publication Ispra 2004 No.73
908 (S.P.I.04.73), European Soil Bureau Research Report. Luxembourg.

909 Knadel, M., Masís-Meléndez, F., De Jonge, L.W., Moldrup, P., Arthur, E., Greve, M.H., 2016.
910 Assessing Soil Water Repellency of a Sandy Field with Visible near Infrared Spectroscopy:
911 <http://dx.doi.org/10.1255/jnirs.1188> 24, 215–224. <https://doi.org/10.1255/JNIRS.1188>

912 Knisel, W.G., Nicks, A.D., 1981. CREAMS: A Field Scale Model for Chemicals, Runoff, and
913 Erosion from Agriculture Management System, 26th ed, United States. Science and
914 Education Administration. Dept. of Agriculture, Science and Education Administration.

915 Kort, J., Collins, M., Ditsch, D., 1998. A review of soil erosion potential associated with biomass
916 crops. *Biomass and Bioenergy* 14, 351–359. [https://doi.org/10.1016/S0961-9534\(97\)10071-](https://doi.org/10.1016/S0961-9534(97)10071-X)
917 X

918 Krisnayanti, D.S., Bunganaen, W., Frans, J.H., Seran, Y.A., Legono, D., 2021. Curve number
919 estimation for ungauged watershed in semiarid region. *Civ. Eng. J.* 7, 1070–1083.
920 <https://doi.org/10.28991/CEJ-2021-03091711>

921 Krysanova, V., Hattermann, F., Wechsung, F., 2007. Implications of complexity and uncertainty
922 for integrated modelling and impact assessment in river basins. *Environ. Model. Softw.* 22,
923 701–709. <https://doi.org/10.1016/j.envsoft.2005.12.029>

924 Kühn, P., 2003. Micromorphology and Late Glacial/Holocene genesis of Luvisols in
925 Mecklenburg–Vorpommern (NE-Germany). *CATENA* 54, 537–555.
926 [https://doi.org/10.1016/S0341-8162\(03\)00129-2](https://doi.org/10.1016/S0341-8162(03)00129-2)

927 Kusumandari, A., Satriagasa, M.C., Hadi Purwanto, R., Widayanti, W.T., 2021. Erosion
928 Measurement by Using Rainfall Simulator at Grass Soil and after Harvested Soil in
929 Wanagama, in: *IOP Conference Series: Earth and Environmental Science*. IOP Publishing.
930 <https://doi.org/10.1088/1755-1315/810/1/012053>

931 L. D. Meyer, 1981. How Rain Intensity Affects Interrill Erosion. *Trans. ASAE* 24, 1472–1475.
932 <https://doi.org/10.13031/2013.34475>

933 Lasanta, T., García-Ruiz, J.M., Pérez-Rontomé, C., Sancho-Marcén, C., 2000. Runoff and
934 sediment yield in a semi-arid environment: The effect of land management after farmland
935 abandonment. *Catena* 38, 265–278. [https://doi.org/10.1016/S0341-8162\(99\)00079-X](https://doi.org/10.1016/S0341-8162(99)00079-X)

936 Li, T., Zhao, L., Duan, H., Yang, Y., Wang, Y., Wu, F., 2020. Exploring the interaction of
937 surface roughness and slope gradient in controlling rates of soil loss from sloping farmland
938 on the Loess Plateau of China. *Hydrol. Process.* 34, 339–354.
939 <https://doi.org/10.1002/HYP.13588>

- 940 Li, Y., Zhang, F., Yang, M., Zhang, J., Xie, Y., 2019. Impacts of biochar application rates and
941 particle sizes on runoff and soil loss in small cultivated loess plots under simulated rainfall.
942 *Sci. Total Environ.* 649, 1403–1413. <https://doi.org/10.1016/j.scitotenv.2018.08.415>
- 943 Li, Z., Liu, C., Dong, Y., Chang, X., Nie, X., Liu, L., Xiao, H., Lu, Y., Zeng, G., 2017. Response
944 of soil organic carbon and nitrogen stocks to soil erosion and land use types in the Loess
945 hilly–gully region of China. *Soil Tillage Res.* 166, 1–9.
946 <https://doi.org/10.1016/j.still.2016.10.004>
- 947 Li, Z., Yu, X., 2012. Characteristics of surface runoff and its influencing factors on slope scale in
948 rocky mountain area of northern Hebei province. *Nongye Gongcheng Xuebao/Transactions*
949 *Chinese Soc. Agric. Eng.* 28, 109–116. [https://doi.org/10.3969/J.ISSN.1002-](https://doi.org/10.3969/J.ISSN.1002-6819.2012.17.016)
950 [6819.2012.17.016](https://doi.org/10.3969/J.ISSN.1002-6819.2012.17.016)
- 951 Lin, J., Zhu, G., Wei, J., Jiang, F., Wang, M. kuang, Huang, Y., 2018. Mulching effects on
952 erosion from steep slopes and sediment particle size distributions of gully colluvial deposits.
953 *CATENA* 160, 57–67. <https://doi.org/10.1016/J.CATENA.2017.09.003>
- 954 Liu, D., She, D., Yu, S., Shao, G., Chen, D., 2015. Rainfall intensity and slope gradient effects on
955 sediment losses and splash from a saline-sodic soil under coastal reclamation. *Catena* 128,
956 54–62. <https://doi.org/10.1016/j.catena.2015.01.022>
- 957 Liu, Singh, 2004. Effect of Microtopography, Slope Length and Gradient, and Vegetative Cover
958 on Overland Flow through Simulation. *J. Hydrol. Eng.* 9, 375–382.
959 [https://doi.org/10.1061/\(ASCE\)1084-0699\(2004\)9:5\(375\)](https://doi.org/10.1061/(ASCE)1084-0699(2004)9:5(375))
- 960 Liu, Y., Xin, Y., Xie, Y., Wang, W., 2019. Effects of slope and rainfall intensity on runoff and
961 soil erosion from furrow diking under simulated rainfall. *Catena* 177, 92–100.
962 <https://doi.org/10.1016/j.catena.2019.02.004>
- 963 Loch, R.J., 2000. Effects of vegetation cover on runoff and erosion under simulated rain and
964 overland flow on a rehabilitated site on the Meandu Mine, Tarong, Queensland. *Soil Res.*
965 38, 299–312. <https://doi.org/10.1071/SR99030>
- 966 Lu, J., Zheng, F., Li, G., Bian, F., An, J., 2016. The effects of raindrop impact and runoff
967 detachment on hillslope soil erosion and soil aggregate loss in the Mollisol region of
968 Northeast China. *Soil Tillage Res.* 161, 79–85. <https://doi.org/10.1016/J.STILL.2016.04.002>
- 969 M. Sheklabadi, H. Khademi, A. H. Charkhabi, 2012. Runoff and Sediment Yield in Soils
970 Developed on Different Parent Materials in the Golabad Watershed, Ardestan. *J. Sci.*
971 *Technol. Agric. Nat. Resour.* 7, 101–245.
- 972 Meena, R.S., Lal, R., Yadav, G.S., 2020. Long-term impacts of topsoil depth and amendments on
973 soil physical and hydrological properties of an Alfisol in central Ohio, USA. *Geoderma* 363,
974 114164. <https://doi.org/10.1016/J.GEODERMA.2019.114164>
- 975 Meng, Q., Fu, B., Tang, X., Ren, H., 2007. Effects of land use on phosphorus loss in the hilly
976 area of the Loess Plateau, China. *Environ. Monit. Assess.* 2007 1391 139, 195–204.
977 <https://doi.org/10.1007/S10661-007-9826-8>
- 978 Meyer, L.D., Harmon, W.C., 1989. How row-sideslope length and steepness affect sideslope
979 erosion. *Trans. Am. Soc. Agric. Eng.* 32, 639–644. <https://doi.org/10.13031/2013.31050>

- 980 Michel, E., Majdalani, S., Di-Pietro, L., 2014. A novel conceptual framework for long-term
981 leaching of autochthonous soil particles during transient flow. *Eur. J. Soil Sci.* 65, 336–347.
982 <https://doi.org/10.1111/ejss.12135>
- 983 Mohamadi, M.A., Kavian, A., 2015. Effects of rainfall patterns on runoff and soil erosion in field
984 plots. *Int. Soil Water Conserv. Res.* 3, 273–281. <https://doi.org/10.1016/j.iswcr.2015.10.001>
- 985 Nassif, S.H., Wilson, E.M., 1975. The influence of slope and rain intensity on runoff and
986 infiltration. *Hydrol. Sci. Bull.* 20, 539–553. <https://doi.org/10.1080/02626667509491586>
- 987 Nearing, M.A., Simanton, J.R., Norton, L.D., Bulygin, S.J., Stone, J., 1999. Soil erosion by
988 surface water flow on a stony, semiarid hillslope. *Earth Surf. Process. Landforms* 24, 677–
989 686. [https://doi.org/10.1002/\(SICI\)1096-9837\(199908\)24:8<677::AID-ESP981>3.0.CO;2-1](https://doi.org/10.1002/(SICI)1096-9837(199908)24:8<677::AID-ESP981>3.0.CO;2-1)
- 990 Nunes, A.N., de Almeida, A.C., Coelho, C.O.A., 2011. Impacts of land use and cover type on
991 runoff and soil erosion in a marginal area of Portugal. *Appl. Geogr.* 31, 687–699.
992 <https://doi.org/10.1016/J.APGEOG.2010.12.006>
- 993 Ouyang, W., Wu, Y., Hao, Z., Zhang, Q., Bu, Q., Gao, X., 2018. Combined impacts of land use
994 and soil property changes on soil erosion in a mollisol area under long-term agricultural
995 development. *Sci. Total Environ.* 613–614, 798–809.
996 <https://doi.org/10.1016/J.SCITOTENV.2017.09.173>
- 997 P.U., I., A.A., O., O.C., C., I.I., E., M.M., M., 2017. Soil Erosion: A Review of Models and
998 Applications. *Int. J. Adv. Eng. Res. Sci.* 4, 138–150. <https://doi.org/10.22161/ijaers.4.12.22>
- 999 Panagos, P., Katsoyiannis, A., 2019. Soil erosion modelling: The new challenges as the result of
1000 policy developments in Europe. *Environ. Res.* 172, 470–474.
1001 <https://doi.org/10.1016/j.envres.2019.02.043>
- 1002 Pandey, A., Chowdary, V.M., Mal, B.C., 2007. Identification of critical erosion prone areas in the
1003 small agricultural watershed using USLE, GIS and remote sensing. *Water Resour. Manag.*
1004 21, 729–746. <https://doi.org/10.1007/s11269-006-9061-z>
- 1005 Parr, W.C., Taguchi, G., 1989. Introduction to Quality Engineering: Designing Quality into
1006 Products and Processes. *Technometrics* 31, 255. <https://doi.org/10.2307/1268824>
- 1007 Peng, T., Wang, S. jie, 2012. Effects of land use, land cover and rainfall regimes on the surface
1008 runoff and soil loss on karst slopes in southwest China. *CATENA* 90, 53–62.
1009 <https://doi.org/10.1016/J.CATENA.2011.11.001>
- 1010 Poulénard, J., Podwojewski, P., Janeau, J.L., Collinet, J., 2001. Runoff and soil erosion under
1011 rainfall simulation of Andisols from the Ecuadorian Páramo: Effect of tillage and burning.
1012 *Catena* 45, 185–207. [https://doi.org/10.1016/S0341-8162\(01\)00148-5](https://doi.org/10.1016/S0341-8162(01)00148-5)
- 1013 Rainfall simulator - Field measurement equipment | Eijkelkamp [WWW Document], 2018. URL
1014 <https://en.eijkelkamp.com/products/field-measurement-equipment/rainfall-simulator.html>
1015 (accessed 10.20.21).
- 1016 Ramezanpour, H., Esmaeilnejad, L., Akbarzadeh, A., 2010. Influence of soil physical and
1017 mineralogical properties on erosion variations in Marlylands of Southern Guilan Province,
1018 Iran. *Int. J. Phys. Sci.* 5, 365–378. <https://doi.org/10.5897/IJPS.9000311>

- 1019 Ramos, M.C., Lizaga, I., Gaspar, L., Quijano, L., Navas, A., 2019. Effects of rainfall intensity
1020 and slope on sediment, nitrogen and phosphorous losses in soils with different use and soil
1021 hydrological properties. *Agric. Water Manag.* 226, 105789.
1022 <https://doi.org/10.1016/j.agwat.2019.105789>
- 1023 Raza, A., Ahrends, H., Habib-Ur-Rahman, M., Gaiser, T., 2021. Modeling Approaches to Assess
1024 Soil Erosion by Water at the Field Scale with Special Emphasis on Heterogeneity of Soils
1025 and Crops. *L.* 2021, Vol. 10, Page 422 10, 422. <https://doi.org/10.3390/LAND10040422>
- 1026 Renard, K.G., Foster, G.R., Weesies, G.A., Porter, J.P., 1991. RUSLE: revised universal soil loss
1027 equation. *J. Soil Water Conserv.* 46, 30–33.
- 1028 Rieke-Zapp, D.H., Nearing, M.A., 2005. Slope Shape Effects on Erosion: A Laboratory Study.
1029 *Soil Sci. Soc. Am. J.* 69, 1463–1471. <https://doi.org/10.2136/sssaj2005.0015>
- 1030 Roth, C.H., Vieira, M.J., Derpsch, R., Meyer, B., Frede, H. -G, 1987. Infiltrability of an Oxisol in
1031 Paraná, Brazil as Influenced by Different Crop Rotations. *J. Agron. Crop Sci.* 159, 186–191.
1032 <https://doi.org/10.1111/j.1439-037X.1987.tb00084.x>
- 1033 Sadeghi, S.H., Kiani Harchegani, M., Asadi, H., 2017. Variability of particle size distributions of
1034 upward/downward splashed materials in different rainfall intensities and slopes. *Geoderma*
1035 290, 100–106. <https://doi.org/10.1016/j.geoderma.2016.12.007>
- 1036 Sepaskhah, A.R., Bazrafshan-Jahromi, A.R., 2006. Controlling Runoff and Erosion in Sloping
1037 Land with Polyacrylamide under a Rainfall Simulator. *Biosyst. Eng.* 93, 469–474.
1038 <https://doi.org/10.1016/j.biosystemseng.2006.01.003>
- 1039 Sharpley, A., Kleinman, P., 2003. Effect of Rainfall Simulator and Plot Scale on Overland Flow
1040 and Phosphorus Transport. *J. Environ. Qual.* 32, 2172–2179.
1041 <https://doi.org/10.2134/jeq2003.2172>
- 1042 Sivaiah, P., Chakradhar, D., 2019. Modeling and optimization of sustainable manufacturing
1043 process in machining of 17-4 PH stainless steel. *Meas. J. Int. Meas. Confed.* 134, 142–152.
1044 <https://doi.org/10.1016/j.measurement.2018.10.067>
- 1045 Sosa-Pérez, G., MacDonald, L.H., 2017. Effects of closed roads, traffic, and road
1046 decommissioning on infiltration and sediment production: A comparative study using
1047 rainfall simulations. *CATENA* 159, 93–105.
1048 <https://doi.org/10.1016/J.CATENA.2017.08.004>
- 1049 Srinivasan, M.S., Kleinman, P.J.A., Sharpley, A.N., Buob, T., Gburek, W.J., 2007. Hydrology of
1050 Small Field Plots Used to Study Phosphorus Runoff under Simulated Rainfall. *J. Environ.*
1051 *Qual.* 36, 1833–1842. <https://doi.org/10.2134/jeq2007.0017>
- 1052 Sukartaatmadja, S., Sato, Y., Yamaji, E., Ishikawa, M., 2003. The Effect of Rainfall Intensity on
1053 Soil Erosion and Runoff for Latosol Soil in Indonesia. *Indones. J. Agron.* 31.
1054 <https://doi.org/10.24831/jai.v31i2.1469>
- 1055 Sun, L., Zhou, J.L., Cai, Q., Liu, S., Xiao, J., 2021. Comparing surface erosion processes in four
1056 soils from the Loess Plateau under extreme rainfall events. *Int. Soil Water Conserv. Res.* 9,
1057 520–531. <https://doi.org/10.1016/J.ISWCR.2021.06.008>
- 1058 Syvitski, J.P.M., Kettner, A.J., 2008. Scaling sediment flux across landscapes. *IAHS-AISH Publ.*

- 1059 149–156.
- 1060 Taguchi, G., 1987. *The System of Experimental Design: Engineering Methods to Optimize*
1061 *Quality and Minimize Costs*, 1st ed, Response. Quality Resources.
- 1062 Taguchi, G., 1986. *Introduction to quality engineering : designing quality into products and*
1063 *processes*. Quality Resources.
- 1064 Tong Li, Dong, J., Yuan, W., 2020. Effects of Precipitation and Vegetation Cover on Annual
1065 Runoff and Sediment Yield in Northeast China: A Preliminary Analysis. *Water Resour.* 47,
1066 491–505. <https://doi.org/10.1134/S0097807820030173/FIGURES/10>
- 1067 Václavík, T., Lautenbach, S., Kuemmerle, T., Seppelt, R., 2013. Mapping global land system
1068 archetypes. *Glob. Environ. Chang.* 23, 1637–1647.
1069 <https://doi.org/10.1016/j.gloenvcha.2013.09.004>
- 1070 Van Dijk, P.M., Van Der Zijp, M., Kwaad, F.J.P.M., 1996. Soil erodibility parameters under
1071 various cropping systems of maize. *Hydrol. Process.* 10, 1061–1067.
1072 [https://doi.org/10.1002/\(SICI\)1099-1085\(199608\)10:8<1061::AID-HYP411>3.0.CO;2-V](https://doi.org/10.1002/(SICI)1099-1085(199608)10:8<1061::AID-HYP411>3.0.CO;2-V)
- 1073 Viney, N.R., Sivapalan, M., 1999. A conceptual model of sediment transport: Application to the
1074 Avon River Basin in Western Australia. *Hydrol. Process.* 13, 727–743.
1075 [https://doi.org/10.1002/\(SICI\)1099-1085\(19990415\)13:5<727::AID-HYP776>3.0.CO;2-D](https://doi.org/10.1002/(SICI)1099-1085(19990415)13:5<727::AID-HYP776>3.0.CO;2-D)
- 1076 Wang, Y., Fan, J., Cao, L., Liang, Y., 2016. Infiltration and Runoff Generation Under Various
1077 Cropping Patterns in the Red Soil Region of China. *L. Degrad. Dev.* 27, 83–91.
1078 <https://doi.org/10.1002/ldr.2460>
- 1079 Warrington, D., Shainberg, I., Agassi, M., Morin, J., 1989. Slope and Phosphogypsum's Effects
1080 on Runoff and Erosion. *Soil Sci. Soc. Am. J.* 53, 1201–1205.
1081 <https://doi.org/10.2136/sssaj1989.03615995005300040035x>
- 1082 Wu, L., Peng, M., Qiao, S., Ma, X. yi, 2018a. Effects of rainfall intensity and slope gradient on
1083 runoff and sediment yield characteristics of bare loess soil. *Environ. Sci. Pollut. Res.*
1084 <https://doi.org/10.1007/s11356-017-0713-8>
- 1085 Wu, L., Qiao, S., Peng, M., Ma, X., 2018b. Coupling loss characteristics of runoff-sediment-
1086 adsorbed and dissolved nitrogen and phosphorus on bare loess slope. *Environ. Sci. Pollut.*
1087 *Res.* 25, 14018–14031. <https://doi.org/10.1007/s11356-018-1619-9>
- 1088 Yan, Y., Dai, Q., Yuan, Y., Peng, X., Zhao, L., Yang, J., 2018. Effects of rainfall intensity on
1089 runoff and sediment yields on bare slopes in a karst area, SW China. *Geoderma* 330, 30–40.
1090 <https://doi.org/10.1016/j.geoderma.2018.05.026>
- 1091 Yost, J.L., Hartemink, A.E., 2019. Soil organic carbon in sandy soils: A review. *Adv. Agron.*
1092 158, 217–310. <https://doi.org/10.1016/BS.AGRON.2019.07.004>
- 1093 Yusuf, K., Omokore, S., Oyebo, O., Adebayo, K., 2016. Effect of vegetative cover and slope
1094 on soil loss by erosion using rainfall simulator. *J. Res. For. Wildl. Environ.* 8, 45–52.
- 1095 Zambon, N., Johannsen, L.L., Strauss, P., Dostal, T., Zúmr, D., Cochrane, T.A., Klik, A., 2021.
1096 Splash erosion affected by initial soil moisture and surface conditions under simulated
1097 rainfall. *Catena* 196, 104827. <https://doi.org/10.1016/j.catena.2020.104827>

- 1098 Zapata, N., Salvador, R., Latorre, B., Paniagua, P., Medina, E.T., Playán, E., 2021. Effect of a
1099 growing maize canopy on solid-set sprinkler irrigation: kinetic energy dissipation and water
1100 partitioning. *Irrig. Sci.* 39, 329–346. [https://doi.org/10.1007/S00271-020-00713-](https://doi.org/10.1007/S00271-020-00713-Z)
1101 [Z/FIGURES/10](https://doi.org/10.1007/S00271-020-00713-Z)
- 1102 Zhang, F., Yang, M., Li, Z., 2015. Feasibility analysis of replacing full factorial design with
1103 Taguchi method in mini-plot soil erosion experiments. *Nongye Gongcheng*
1104 *Xuebao/Transactions Chinese Soc. Agric. Eng.* 31, 1–9.
1105 <https://doi.org/10.11975/J.ISSN.1002-6819.2015.13.001>
- 1106 Zhang, J.H., Wang, Y., Li, F.C., 2015. Soil organic carbon and nitrogen losses due to soil erosion
1107 and cropping in a sloping terrace landscape. *Soil Res.* 53, 87–96.
1108 <https://doi.org/10.1071/SR14151>
- 1109 Zhao, Q., Li, D., Zhuo, M., Guo, T., Liao, Y., Xie, Z., 2015. Effects of rainfall intensity and slope
1110 gradient on erosion characteristics of the red soil slope. *Stoch. Environ. Res. Risk Assess.*
1111 29, 609–621. <https://doi.org/10.1007/S00477-014-0896-1>/[FIGURES/6](https://doi.org/10.1007/S00477-014-0896-1)
- 1112 Zhong, R.-L., Zhang, P.-C., 2011. Experimental Study on Characteristics of Runoff and Erosional
1113 Sediment Yield on Purple Soil Slope. *J. yangtze river Sci. Res. Inst.* 28, 22–27.
- 1114 Ziadat, F.M., Taimeh, A.Y., 2013a. Effect of rainfall intensity, slope, land use and antecedent soil
1115 moisture on soil erosion in an arid environment. *L. Degrad. Dev.* 24, 582–590.
1116 <https://doi.org/10.1002/ldr.2239>
- 1117 Ziadat, F.M., Taimeh, A.Y., 2013b. Effect of rainfall intensity, slope, land use and antecedent soil
1118 moisture on soil erosion in an arid environment. *L. Degrad. Dev.* 24, 582–590.
1119 <https://doi.org/10.1002/ldr.2239>
- 1120 Zuazo, V.H.D., Pleguezuelo, C.R.R., 2008. Soil-erosion and runoff prevention by plant covers. A
1121 review. *Agron. Sustain. Dev.* <https://doi.org/10.1051/agro:2007062>
- 1122